NASA TECHNICAL NOTE

NASA TN D-4686

EFFECT OF HINGE-LINE BLEED ON HEAT TRANSFER AND PRESSURE DISTRIBUTION OVER A WEDGE-FLAP COMBINATION AT MACH 10.4

by H. Harris Hamilton and J. David Dearing

Langley Research Center
Langley Station, Hampton, Va.

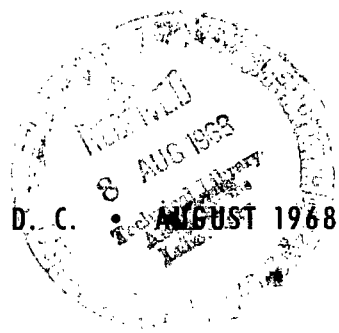

NATIONAL AERONAUTICS AND SPACE ADMINISTRATION • WASHINGTON, D. C. • AUGUST 1968

EFFECT OF HINGE-LINE BLEED ON HEAT TRANSFER AND PRESSURE DISTRIBUTION OVER A WEDGE-FLAP COMBINATION AT MACH 10.4

By H. Harris Hamilton and J. David Dearing

Langley Research Center
Langley Station, Hampton, Va.

NATIONAL AERONAUTICS AND SPACE ADMINISTRATION

For sale by the Clearinghouse for Federal Scientific and Technical Information
Springfield, Virginia 22151 – CFSTI price $3.00

EFFECT OF HINGE-LINE BLEED ON HEAT TRANSFER AND PRESSURE DISTRIBUTION OVER A WEDGE-FLAP COMBINATION AT MACH 10.4

By H. Harris Hamilton and J. David Dearing
Langley Research Center

SUMMARY

An experimental investigation has been conducted to determine the effect of boundary-layer bleed on the heat transfer and pressure distributions over a wedge-flap combination with a gap between the wedge and flap. The model was tested, with the wedge at angles of attack of 6.83° and 12.83° and the flap deflected up to 30°, at a nominal free-stream Mach number of 10.4 and free-stream Reynolds numbers (based on distance to the flap hinge line) of 0.8×10^6 and 3.6×10^6.

At the lower free-stream Reynolds number, the boundary layer was laminar over the entire model. Under this condition an extensive separated region was observed for all flap deflections when the gap was sealed. Opening the gap decreased the extent of separation, but for the larger flap deflections the separated region was never entirely eliminated. The pressure and heat transfer over the forward portion of the flap increased slightly as the gap size increased.

At the higher free-stream Reynolds number, the boundary layer was transitional at the hinge line for an angle of attack of 6.83° and was fully turbulent for an angle of attack of 12.83°. Under these conditions, the largest flap deflection of the tests did not separate the boundary layer even with the gap sealed, and increasing the gap size had very little effect on either the pressure or heat-transfer distributions.

The turbulent heat-transfer rate for deflected flap was predicted reasonably well by the Spalding and Chi turbulent theory by using boundary-layer-edge properties calculated from oblique shock theory and by assuming that the turbulent boundary layer originated at the flap hinge line.

INTRODUCTION

In the design of high-speed vehicles such as various lifting body reentry configurations or hypersonic-cruise aircraft, the designer is faced with the solution of problems associated with boundary-layer separation forced by deflected control surfaces. The

onset of this type of separation can bring about large and sudden changes in vehicle flight characteristics and can also produce large increases in the local aerodynamic heating on the control surface. (See refs. 1 to 3.)

The body of theoretical and experimental studies of high-speed separation phenomenon has grown over the past decade (for example, see refs. 4 to 23) until at present the designer has available both semiempirical correlations and theories for calculating some of the more important separation characteristics. These studies have, in general, been restricted to the case of two-dimensional or axial-symmetrical "free-interaction" separation with no mass bleed from the separation "bubble."

Extensive mass bleed from separation bubbles on flight vehicles can occur because of lateral flow around the edges of low-aspect-ratio flap-type controls. The effect of this type of mass bleed on the pressure distribution is discussed in references 2 and 24.

Various practical considerations may make it difficult to seal the gap completely between the flap and main body of the vehicle, and thus it is possible that the separation bubble will be vented to a low-pressure region on a leeward surface. The effect on the external flow of this type of mass bleed has been investigated by Crawford (ref. 25), and more recently, by Stern and Rowe (ref. 26). Crawford used an ogive-cylinder conical-flare model with a gap at the junction between the cylinder and flare. He investigated the effect of both radial and axial bleed on the flow field and on the heat-transfer distributions on the flare. Stern and Rowe used a blunt delta wing with a trailing-edge flap to study the effect of bleed through a hinge-line gap on the external flow and on the flow through the gap. The complex flow field about the blunt delta wing makes it difficult to compare the results of that investigation with those for the more nearly two-dimensional investigations conducted previously (that is, refs. 4 to 23).

The present investigation was undertaken to clarify the problems associated with mass bleed through gaps at the hinge line of two-dimensional flap-type controls and its influence on the external flow. The model used in the present investigation is a slender two-dimensional wedge-flap combination with a gap between the wedge and flap.

Pressure and heat-transfer measurements were made on the wedge and on the surface of the flap. The model was tested at angles of attack of 6.83° and 12.83° (to produce the pressure differential across the gap that is necessary to bleed mass from the flow field) with the trailing-edge flap deflected at 0°, 10°, 20°, and 30°. The tests were conducted with various gap sizes at free-stream Reynolds numbers, based on distance to the hinge line, of 0.8×10^6 and 3.6×10^6 and a nominal free-stream Mach number of 10.4.

SYMBOLS

A,B	gap entrance or exit width (see fig. 3(b))
c_p	specific heat at constant pressure
c_w	specific heat of wall material
C_f	skin-friction coefficient, $\frac{\tau_w}{\frac{1}{2}\rho U^2}$
$C_{p,p}$	plateau pressure coefficient, $\frac{p_p - p_o}{\frac{1}{2}\rho_o U_o^2}$
h	heat-transfer coefficient, $\frac{q_w}{T_{aw} - T_w}$
k_w	heat conductivity of wall material
K	height of surface roughness
L	surface distance from leading edge to hinge line
M	Mach number
N_{Pr}	Prandtl number
N_{St}	Stanton number, $\frac{h}{\rho U c_p}$
p	pressure
q	rate of heat flow per unit area
q_c	net rate of heat flow resulting from conduction per unit surface area
r_1	radius of flap leading edge (see fig. 3(b))
r_2	radius of cove surface (see fig. 3(b))
R	unit Reynolds number, $\frac{\rho U}{\mu}$

$R_{\infty,L}$	free-stream Reynolds number based on distance to hinge line, $\frac{\rho_\infty U_\infty L}{\mu_\infty}$
$R_{\infty,x}$	free-stream Reynolds number based on distance from leading edge, $\frac{\rho_\infty U_\infty x}{\mu_\infty}$
$R_{l,L}$	local Reynolds number based on distance to hinge line, $\frac{\rho_l U_l L}{\mu_l}$
$R_{l,x}$	local Reynolds number based on distance from leading edge, $\frac{\rho_l U_l x}{\mu_l}$
t	time
T	temperature
U	velocity
x	longitudinal surface distance measured from leading edge
x_s	separation point, assumed to be located where $\frac{p}{p_\infty} = \frac{1}{2}\left(\frac{p_p + p_o}{p_\infty}\right)$
y	lateral surface distance measured from model center line
α	angle of attack of windward surface, positive with nose up (see fig. 3(a))
γ	ratio of specific heats
δ^*	boundary-layer displacement thickness
δ_f	flap deflection angle
λ_w	wall thickness
ϵ	gap size
η	temperature recovery factor, $\frac{T_{aw} - T_l}{T_t - T_l}$
ρ	density of fluid
ρ_w	density of wall material

τ_w shear stress at wall

μ dynamic viscosity of air

Subscripts:

aw adiabatic wall

l local

o local conditions at beginning of interaction

p plateau

r reattachment

s separation

t total

w wall

∞ free-stream conditions

Primes denote properties evaluated at reference temperature.

FACILITY

The tests were conducted in the nominal Mach 10.4 nozzle of the Langley continuous-flow hypersonic tunnel. The test air is heated in an electrical resistance tube heater prior to expansion through the nozzle to avoid liquefaction in the test section. The nozzle is contoured and water cooled, and has a 31-inch (78.7 cm) square test section. A more detailed description of the facility and its operation is given in reference 27.

A calibration of the Mach 10.4 nozzle equipped with a beryllium-copper throat is shown in figure 1. The data symbols represent average Mach number in the test-section core, whereas the brackets on the symbols represent the range of variation of Mach number over the test-section core.

MODEL

General Description

The model used in this investigation is shown in the photograph in figure 2 and the sketch in figure 3(a). It was a 5.67° wedge the sides of which were swept inward toward the trailing edge at the free-stream Mach angle to minimize the base area and thus the probability of tunnel blockage. The leading edge had a thickness of approximately 0.001 inch (0.00254 cm) and was beveled at an angle of 20° toward the uninstrumented side of the model. (See detail of leading edge in fig. 3(a).) A flap with a 6-inch (21.24 cm) chord and 6-inch (21.24 cm) span was located at the rear of the model. The flap could be set at angular deflection from -40° to 40°. Sharp-edged end plates were located on either side of the flap and extended from approximately 7 inches (17.78 cm) upstream of the hinge line to the trailing edge on both the upper and lower surfaces of the model. Their primary purpose was to minimize spanwise flow on the flap, but they also prevented disturbances created by the strut from feeding on to the instrumented portion of the model.

There was a gap between the wedge and the flap. (See detailed sketch in fig. 3(b).) The width of the gap was controlled by the position of a movable section of the wedge body upstream of the flap hinge line. The radii of both the cove surface and the flap surface were fixed; thus, the distribution of area in the gap changed with each gap setting as is shown in the table in figure 3(b). The term gap size ϵ as it will be used here refers to the distance between the gap walls along the plane of symmetry of the wedge. Gap sizes of 0.0625, 0.125, 0.250, and 0.500 inch (0.1588, 0.3175, 0.6350, and 1.2700 cm) were tested. A seal (shown in fig. 3(b)) could be attached to the uninstrumented side of the model near the gap exit to prevent flow through the gap. The seal was used only with the 0.0625-inch (0.1588 cm) gap. Most of the tests were conducted with a sharp section forming the upstream boundary of the gap; however, tests were also conducted with a rounded lip to determine whether rounding of the lip had any effect on the pressure or heat-transfer distributions. (See sketch in fig. 3(b).)

The wedge was constructed of thin sections of inconel skin, approximately 0.030 inch (0.0762 cm) thick, fastened over a wedge-shaped ribbed understructure. The wedge skin was attached to the understructure by countersunk screws. (See fig. 2.) The flap was constructed by electron beam welding a thin section of inconel skin over a ribbed frame. The high skin temperature $T_w \approx 1000^\circ$ F (811° K) encountered on the flap when testing at the larger flap deflections coupled with this type of construction (that is, a thin expanding skin restrained by a more massive and thus cooler understructure) caused the flap surface to become permanently distorted. A photograph of the distorted surface of the flap taken after completion of the tests is shown in figure 4. The amplitude of the

most severe distortion was approximately 0.03 inch (0.0762 cm), whereas the distance between peaks varied from 1.5 inches (3.81 cm) to 2.0 inches (5.08 cm). A discussion of the possible effect of these surface distortions on the data is reserved for a later part of this paper when the data are presented and analyzed.

Instrumentation

The model was equipped with 32 no. 30-gage, chromel-alumel glass-insulated thermocouples for measurement of model surface temperature. The thermocouples were spotwelded to the back side of the lower surface in rows, 1 inch (2.54 cm) on either side of the center line. Pressure orifices (0.060-inch-diameter (0.152 cm)) were located along the center line of the lower model surface. Each orifice was connected to either an ionization gage or a strain-gage pressure transducer. The detailed location of both the thermocouples and pressure orifices is given in table I. The accuracy of the ionization gages is ±2 percent of reading for pressures from approximately 0.02 to 0.60 psia (0.14 to 4.1×10^3 N/m^2) and ±5 percent of the measured pressure for pressures below approximately 0.02 psia (0.14×10^3 N/m^2). The accuracy of the strain-gage transducers is better than ±0.25 percent of full-scale reading for the 1 psi (6.89×10^3 N/m^2) and 3 psi (20.7×10^3 N/m^2) instruments, and ±0.50 percent of full-scale reading for the 10 psi (68.9×10^3 N/m^2) and 15 psi (103×10^3 N/m^2) instruments. The outputs from both the thermocouples and pressure instruments were automatically recorded on magnetic tape during the tests by using an analog-to-digital converter and data-recording system.

TESTS AND PROCEDURES

The nominal test conditions are given in the following table:

p_t		T_t		M_∞	p_∞		T_∞		R_∞	
psia	N/m^2	$^\circ$R	$^\circ$K		psia	N/m^2	$^\circ$R	$^\circ$K	1/ft	1/m
300	20.7×10^5	1760	978	10.18	0.00606	41.8	84.2	46.8	0.41×10^6	1.35×10^6
1500	103.5×10^5	1840	1022	10.48	0.02550	175.9	84.2	46.8	1.79×10^6	5.87×10^6

The free-stream quantities listed were calculated by using the real-gas relations given by Erickson and Creekmore (ref. 28). The parameters varied at each stagnation pressure are given in table II.

Prior to testing, the models were positioned in a closed chamber mounted on the side wall of the tunnel and cooled to approximately room temperature with high-pressure

air jets. The model was then injected into the hypersonic airstream and data were automatically recorded at intervals of 0.05 second. The data necessary for obtaining the heat-transfer rates were generally recorded within 2 seconds after injection; however, the model was exposed to hypersonic flow up to an additional 15 seconds to allow transients in the indicated pressure to settle out.

REDUCTION OF HEAT-TRANSFER DATA

The heat transfer was obtained by the transient calorimeter technique for which the heat-transfer rate is assumed to be equal to the rate of heat stored in the surface; thus,

$$q = h\left(T_{aw} - T_w\right) = \rho_w \lambda_w c_w \frac{dT_w}{dt}$$

The heat-transfer rates were obtained before the surface heated up significantly; thus, radiation from the surface was negligible. The derivative in this equation was obtained from a least-squares curve fit to a 1- or 2-second interval of recorded temperatures and was evaluated at the center of the interval. The density and the specific heat of inconel were taken from reference 29. The adiabatic wall temperature at each thermocouple location was calculated from the following equation:

$$\frac{T_{aw}}{T_t} = \eta + \frac{T_l}{T_t}(1 - \eta)$$

for a laminar recovery factor η (assumed to be 0.84). The use of a turbulent recovery factor ($\eta = 0.89$) would have lowered the heat-transfer results by a maximum of 8 percent. The local static temperature was determined from inviscid oblique-shock theory (ref. 30) by assuming the air in the test section to behave as a perfect gas with $\gamma = 1.4$.

Estimates of a surface conduction error in the measured heat-transfer rates were made by using the equation:

$$q_c = k_w \frac{d^2 T_w}{dx^2}$$

The derivative in this equation was evaluated from faired distributions of wall temperature by using a three-point finite-difference technique. With the use of this method, the calculated conduction correction was less than 2 percent of the measured heating rate except at the tangent point (see fig. 3(b)) on the flap hinge line; here, the calculated conduction correction was as high as 20 percent of the measured heating rate for the tests with $R_{\infty,L} = 3.6 \times 10^6$ and $\delta_f = 30^o$. The heat-transfer data are presented without conduction corrections.

RESULTS AND DISCUSSION

Flow Model

A simplified model for the flow over a flap with a gap upstream of the hinge line is shown in figure 5. With the gap sealed, the flow pattern is similar to that for the free-interaction separation model upstream of a compression corner with no mass bleed (discussed, for example, in refs. 4 and 8). If the existence of steady flow is assumed, the dividing streamline leaves the surface at the separation point x_s and returns to the surface at the reattachment point x_r. Separation occurs as the result of interaction between the boundary-layer growth and the external inviscid flow (ref. 4). The pressure and heat-transfer distributions for this situation are similar to those for flow with no hinge-line gap.

Crawford (ref. 25) has shown that bleeding a small amount of mass through the gap reduces the size of the separated region. This case is depicted in figure 5(b). The characteristics of the flow near separation are similar to the case previously described, but flow in reattachment region is considerably altered. The existence of a steady separated region requires that the streamline leaving the surface at the separation point x_s return to the same surface at the upstream lip of the gap $(x_r)_1$. The streamline which reattaches to the flap at $(x_r)_2$ passes above the wall at the separation point x_s and the fluid enclosed between these two streamlines must pass through the gap. (See fig. 5(b).) When a large amount of fluid is bled from the boundary layer, a separated region probably will not form upstream of the hinge line. This case is shown in figure 5(c). A streamline attaches to the flap at x_r and all the fluid beneath this streamline passes through the gap. Which of these flow fields will exist with an open gap will depend on many factors. In general, the strong influence of any parameter which tends to depress separation with no gap present, such as a turbulent boundary layer, will, when combined with mass bleed, tend to collapse the separation completely as shown in figure 5(c). At the lower Reynolds number $\left(R_{\infty,L} = 0.8 \times 10^6\right)$ in these tests, the boundary layer was probably laminar over the entire model, whereas at the higher Reynolds number $\left(R_{\infty,L} = 3.6 \times 10^6\right)$ the boundary layer was fully turbulent near the hinge line. Since the results obtained at these two free-stream Reynolds numbers are characteristically different, they are presented separately.

Laminar Separation

Pressure and heat-transfer distributions for $R_{\infty,L} = 0.8 \times 10^6$ and $\alpha = 6.83^\circ$ $\left(R_{l,L} = 1.18 \times 10^6,\ M_l = 7.7\right)$ are presented in figure 6 for several flap deflections δ_f and ratios of gap size to flap leading-edge radius ϵ/r_1. For this angle of attack, the ratio of the theoretical pressure on the windward surface of the wedge to that on the leeward surface is approximately 4.95. Flap deflections were limited to 20° at this Reynolds

number because it was not possible to maintain hypersonic flow in the test section for larger flap deflections. All the laminar data were obtained with the use of the gap configuration with a sharp lip.

With the gap sealed, figure 6(a), and $\delta_f = 0^o$, the pressure distribution is predicted reasonably well by the viscous interaction theory of Bertram (ref. 31) and the heat-transfer data are in reasonably good agreement with laminar flat-plate theory (described in the appendix). The boundary layer apparently remains laminar over the entire model. There is little evidence that the distortion of the flap surface noted previously (see fig. 4) had any strong effect on the heat-transfer distributions as in the investigation by Bertram, et al. (ref. 32). The most severe distortion encountered in the present tests was much less than the smallest distortion investigated by Bertram, et al.; thus, these distortions were probably not severe enough to cause local boundary-layer separation.

When the flap is deflected 10^o, the pressure distribution upstream of the hinge line forms a plateau which is characteristic of laminar separation. The separation point is assumed to occur approximately midway up the rise to the plateau pressure (ref. 33). The pressure on the flap increases toward the trailing edge to a value slightly below inviscid theory (ref. 30). The heat transfer in the separated region upstream of the hinge line is below that for attached flow (that is, for $\delta_f = 0^o$). On the flap, the heating increases and reachs a maximum value near the trailing edge. Increasing the flap deflection to 20^o increases the extent of separation and the level of pressure and heat transfer on the flap; however, both the pressure and heat-transfer distributions are qualitatively similar to those obtained with $\delta_f = 10^o$. The overall characteristics of the flow, with a sealed gap, are similar to those observed previously by others, such as Miller, et al. (ref. 9), for laminar separation in a compression corner.

The data obtained with ϵ/r_1 equal to 0.052 are presented in figure 6(b). For this condition, the gap opening is approximately 20 percent of the total boundary-layer thickness on the wedge ahead of the gap entrance. The pressure and heat-transfer distributions are almost identical with those for a sealed gap, presented in figure 6(a), except that for $\delta_f = 20^o$ the heat transfer tends to level off near the trailing edge of the flap. The separation point probably shifts downstream slightly, but this shift cannot be accurately defined because of the sparsity of instrumentation ahead of the hinge line. The flow field for this case should be qualitatively similar to that shown in figure 5(b).

The data shown in figure 6(c) were obtained by increasing the gap size so that $\epsilon/r_1 = 0.208$. For this condition the gap opening is approximately 75 percent of the total boundary-layer thickness ahead of the gap entrance. The pressure and heat-transfer distributions indicate that for $\delta_f = 10^o$, there is little or no boundary-layer separation. For $\delta_f = 20^o$, separation does occur but the separated region is somewhat smaller than that observed previously with the smaller gap. The final pressure on the flap very closely

approaches inviscid theory for both flap deflections. The heat transfer over much of the forward portion of the flap is as much as twice that for the smaller gaps. For $\delta_f = 20^o$, the heating reaches a peak upstream of the trailing edge of the flap. This increase in heating is probably the result of earlier boundary-layer reattachment on the flap.

The effect of gap size and flap deflection on distance from the separation point to the hinge line $\frac{L - x_s}{L}$ is summarized in figure 7. For $\delta_f = 10^o$, increasing the gap size eventually eliminated separation; however, for $\delta_f = 20^o$, the extent of separation was reduced less than 25 percent for the largest gap size tested. Also shown in this figure is the separation length calculated from a semiempirical method by Needham and Stollery (ref. 15) for laminar flow in a compression corner. The agreement with the sealed gap data from the present tests is only fair. (It should be noted that separation length can be affected by flap length.)

In the qualitative discussion of the flow model, it was pointed out that when an extensive region of separation exists, even with mass bleed near the hinge line, the mechanism producing separation should be similar to that proposed by Chapman, et al. (ref. 4). If this is the case, the previous correlations of plateau pressure coefficients should hold for the present data. Figure 8 shows reasonably good agreement of the plateau pressure coefficients from the present tests with those calculated from a semiempirical equation presented by Sterrett and Holloway (ref. 10)

$$\frac{C_{p,p}}{\sqrt{C_{f,o}}} = \frac{2.61 M_o^{-1/4}}{\left(M_o^2 - 1\right)^{1/2}}$$

This relationship has been shown to agree well with unvented separation data at Mach numbers up to approximately 13. Since the plateau coefficients obtained in the present investigation agree reasonably well with those calculated from the preceding equation (previously applied only to separated flows with no mass bleed), it at least suggests that for cases where the region of separation is extensive, venting the separation bubble does not significantly alter the mechanism producing separation (that is, free interaction between the boundary-layer growth and the external inviscid flow). However, more data covering a wider range of test conditions are needed to establish this point firmly.

Transitional and Turbulent Flow

Transitional flow.- The data presented in figure 9 show the effect of flap deflection δ_f and gap size ϵ/r_1 on the pressure and heat-transfer distributions for $R_{\infty,L} = 3.6 \times 10^6$ $\left(R_{l,L} = 5.3 \times 10^6\right)$. The data were obtained by using the sharp-lip gap configuration shown in figure 3(b) with the model at an angle of attack of 6.83^o $\left(M_l \approx 7.9\right)$.

The data presented in figure 9(a) were obtained with the gap sealed. If the heat-transfer data for $\delta_f = 0^o$ are compared with laminar flat-plate theory, it is evident that transition starts well upstream of the hinge line. On the rear of the flap, the heating rates are in reasonably good agreement with Spalding and Chi turbulent theory (described in the appendix) and indicate that the boundary layer is fully turbulent. At the flap hinge line, however, the boundary layer is still transitional.

Upstream of the hinge line the heating is significantly higher on the inboard row of thermocouples (that is, the row shown closest to the strut in fig. 3(b)). Results from oil-flow tests show no evidence of lateral disturbances feeding on to the model which might cause such a disparity. A step discontinuity in the model surface near the leading edge, where the first section of model skin is attached to the understructure (see fig. 2), was discovered after completion of the tests. The ratio of roughness (step) height to the calculated boundary-layer displacement thickness K/δ^* ahead of the inboard row of thermocouples was approximately 0.11, whereas for the other row, $K/\delta^* \approx 0.03$. The relatively larger roughness could have caused earlier transition on the inboard side of the model which would account for the increase in heating. However, previous investigations at lower hypersonic Mach numbers have shown that small roughness heights relative to the boundary-layer thickness have very little effect on transition location. Since it was felt that the heat-transfer rates obtained from the outboard row of thermocouples upstream of the hinge line was probably least disturbed by the roughness, these data have been faired on the figures. On the flap, however, the heating along both rows of instrumentation approaches approximately the same level.

Since at this Reynolds number $\left(R_{\infty,L} = 3.6 \times 10^6\right)$ the boundary layer is transitional at the hinge line, it is not as easily separated as it was at the lower Reynolds number $\left(R_{\infty,L} = 0.8 \times 10^6\right)$ where the boundary layer was laminar. For $\delta_f = 30^o$, a small pressure rise occurs upstream of the hinge line; but it appears that the boundary layer does not separate even for this large flap deflection. The pressure on the flap rises rapidly to the inviscid pressure level and then decreases toward the trailing edge for all flap deflections.

Deflecting the flap has almost no effect on the heat transfer upstream of the hinge line except for $\delta_f = 30^o$ where a small increase in heating is noted close to the hinge line. On the flap the heating increases rapidly and reaches a peak at approximately the same location as the maximum pressure.

The heat transfer to the deflected flap was estimated by the Spalding and Chi turbulent theory (described in the appendix) using boundary-layer edge properties calculated from inviscid theory. The effective origin of the turbulent boundary layer was assumed to be at the flap hinge line (as in refs. 13 and 34). This method considerably

underestimates the heat transfer to the flap for all flap deflections, perhaps because the boundary layer was not fully turbulent ahead of the flap (ref. 13).

The distribution of heating on the flap for $\delta_f = 0^o$ and 10^o is reasonably smooth and regular which suggests that the surface distortion (shown in fig. 4) probably has little effect on the data. For larger flap deflection (that is, $\delta_f = 20^o$ and 30^o), there is some irregularity in the heating distribution near the location of peak heating. The point of highest heating is reasonably consistent with the other data on the flap; thus, the data are faired through this point. The differences in heat-transfer rate near the point of maximum heating could be associated either with the surface distortions or with the nonuniform spanwise location of transition.

The data obtained with ϵ/r_1 equal to 0.052, 0.104, and 0.208 are presented in figures 9(b), 9(c), and 9(d), respectively. Opening the gap (with the flap deflected) reduces the rise in pressure upstream of the hinge line that was noted for the sealed gap in figure 9(a). The open gap has very little effect on either the magnitude or the distribution of the pressure and heat transfer on the flap. This last result is not surprising since Needham and Stollery (ref. 35) have shown, in the case of laminar flow, that it is the high-energy fluid near the outer edge of the boundary layer that has the greatest influence on the flow over a flap. Thus, removing low-energy air from the lower portion of the boundary layer should have little effect on the flow over the flap.

Tests were also conducted at $R_{\infty,L} = 3.6 \times 10^6$ and $\alpha = 6.83^o$ $\left(R_{l,L} = 5.3 \times 10^6, M_l = 7.9\right)$ using the rounded-lip gap configuration shown in figure 3(b). The pressure and heat-transfer distributions from these tests are presented in figure 10. The data in figure 10 were obtained with the use of an open gap with ϵ/r_1 equal to 0.052, 0.208, and 0.416. The boundary layer is transitional at the hinge line; hence, no separation is observed even for $\delta_f = 30^o$. If the data for the various gap sizes (fig. 10) are compared, it is evident that increasing the gap size has little effect on either the pressure or heat-transfer distributions, although a larger gap size $\left(\epsilon/r_1 = 0.416\right)$ was tested with this gap configuration than with the sharp-lip configuration discussed previously.

The effect of lip radius can be ascertained by comparing the data in figures 10(a) and 10(b) with those in figures 9(b) and 9(d), respectively. The rounded lip causes a sharp reduction in the heat transfer and pressure just upstream of the hinge line, but on the flap, the rounded lip has no effect on the heat-transfer or pressure distributions.

Turbulent flow.- The data presented in figure 11 were obtained with a sharp-lip gap configuration at $R_{\infty,L} = 3.6 \times 10^6$ and $\alpha = 12.83^o$ $\left(R_{l,L} = 4.5 \times 10^6, M_l = 5.9\right)$. For this higher angle of attack, the ratio of the theoretical pressure on the windward surface of the wedge to that on the leeward surface is approximately 83.7. When the heat-transfer data for $\delta_f = 0^o$ are compared with laminar and turbulent theory (described in the

appendix), it is evident that transition is completed upstream of the hinge line. The data show no difference between the two rows of thermocouples such as was noted previously at the lower angle of attack (that is, $\alpha = 6.83^{\circ}$). Because of the lower local Mach number combined with the thinner boundary layer (for example, $0.1 \leqq K/\delta^* \leqq 0.3$), the roughness is possibly more effective in causing transition to occur at approximately the same station for each row of thermocouples.

Even for $\delta_f = 20^{\circ}$ (larger flap deflections could not be tested because of tunnel blockage), there is no rise in pressure upstream of the hinge line; thus, the boundary layer is attached. On the flap the pressure rises to the inviscid pressure level and then decreases toward the trailing edge. There is no change in the heating upstream of the hinge line with flap deflection. On the flap, however, the heating increases sharply with δ_f, the distributions qualitatively following those for the pressure. With the boundary layer fully turbulent upstream of the hinge line, the simplified theoretical approach described previously gives a reasonably good prediction of the heat transfer on the deflected flap. (See fig. 11.)

Comparison of the data in figure 11(a) with those in figure 11(b) shows that increasing the gap size has almost no effect on either the pressure or heat-transfer distributions observed on the model.

Tests were also run at these same test conditions and angle of attack, but with the rounded rather than with the sharp-lip gap configuration (fig. 3(b)). These data are shown in figure 12. Upstream of the hinge line there is a decrease in the pressure and heating noted for the rounded-lip gap configuration, but on the flap almost no effect of rounding the lip is noted on either the pressure or heat-transfer distributions. These trends are similar to those noted at the lower angle of attack (that is, $\alpha = 6.83^{\circ}$).

CONCLUDING REMARKS

An experimental investigation has been conducted to determine the pressure and heat-transfer distributions on a wedge-flap combination with a variable size gap between the wedge and flap. The model was tested at angles of attack of 6.83° and 12.83° with the flap deflected up to 30° at a nominal free-stream Mach number of 10.4 and free-stream Reynolds numbers (based on distance to the flap hinge line) of 0.8×10^6 and 3.6×10^6.

At the lower Reynolds number the boundary layer was laminar over the entire model. Under this condition an extensive region of separation was observed for all flap deflections with the gap sealed. Increasing the gap size decreased the extent of separation, but for the larger flap deflections the separated region was never entirely eliminated. The maximum gap width was 75 percent of the calculated boundary-layer thickness at the gap

position. The pressure and heat transfer over the forward portion of the flap increased as the gap size increased.

At the higher free-stream Reynolds number the boundary layer was transitional at the hinge line for an angle of attack of 6.83°. Under these conditions, the largest flap deflections of the test did not separate the boundary layer even with the gap sealed, and increasing the gap size had very little effect on either the pressure or heat-transfer distributions.

The turbulent heat transfer on the deflected flap was predicted reasonably well by the Spalding and Chi turbulent theory by using boundary-layer edge properties calculated from oblique shock theory and assuming that the turbulent boundary layer originated at the flap hinge line.

Langley Research Center,
National Aeronautics and Space Administration,
Langley Station, Hampton, Va., March 21, 1968,
129-01-07-08-23.

APPENDIX A

HEAT-TRANSFER THEORIES

Laminar Theory

Several methods are available for the theoretical calculation of laminar heat transfer. In this analysis the reference-temperature method of Monaghan has been used. The laminar heat-transfer correlating parameter can be written in terms of local reference-temperature conditions by using the Blasius skin friction relation and Reynolds analogy as follows:

$$N'_{St,l}\sqrt{R'_{l,x}} = \frac{0.332}{\left(N'_{Pr}\right)^{2/3}} \tag{A1}$$

The local stream Stanton number and Reynolds number are related to the reference-temperature quantities by

$$N_{St,l} = N'_{St,l}\frac{T_l}{T'_l} \tag{A2}$$

$$R_l = R'_l\frac{\mu'_l T'_l}{\mu_l T_l} \tag{A3}$$

Rewriting the laminar heat-transfer correlating parameter in terms of free-stream conditions yields

$$N_{St,\infty}\sqrt{R_{\infty,x}} = \frac{0.332}{\left(N'_{Pr}\right)^{2/3}}\frac{c_{p,l}}{c_{p,\infty}}\sqrt{\frac{\rho_l}{\rho_\infty}\frac{U_l}{U_\infty}\frac{\mu'_l}{\mu_\infty}}\left(\frac{T_l}{T'_l}\right)^{1/2} \tag{A4}$$

Rewriting the Reynolds number in terms of the characteristic length L results in the following equation:

$$N_{St,\infty}\sqrt{R_{\infty,L}} = \frac{0.332}{\left(N'_{Pr}\right)^{2/3}}\frac{c_{p,l}}{c_{p,\infty}}\sqrt{\frac{\rho_l}{\rho_\infty}\frac{U_l}{U_\infty}\frac{\mu'_l}{\mu_\infty}\frac{T_l}{T'_l}}\left(\frac{L}{x}\right)^{1/2} \tag{A5}$$

Local properties (ρ, T, U, etc.) are calculated from oblique shock theory, the fluid being assumed to behave as a perfect gas with $\gamma = 1.4$, and the reference temperature is calculated from Monaghan's relation for laminar flow (ref. 36)

$$\frac{T'_l}{T_l} = 0.420 + 0.580\frac{T_w}{T_l} + 0.160\frac{\gamma - 1}{2}M_l^2 \tag{A6}$$

APPENDIX A

Turbulent Theory

Theoretical values of turbulent heat transfer were calculated by a modified form of the Spalding and Chi method described in references 37 to 39. The theoretical values of turbulent Stanton number used in the present analysis were calculated directly from the charts and relations presented in reference 39. Boundary-layer edge properties were calculated from oblique shock theory for a perfect gas. For $\delta_f = 0^o$, the virtual origin of the turbulent boundary layer is assumed to be at the point where the boundary layer first becomes fully turbulent as indicated by the maximum heat-transfer rate (ref. 38). When the turbulent heat transfer to the deflected flap is estimated, the turbulent boundary layer is assumed to have the virtual origin at the flap hinge line.

REFERENCES

1. Kaufmann, Louis G., II; Hartofilis, Stavros A.; Evans, William J.; Oman, Richard A.; Meckler, Lawrence H.; and Weiss, Daniel: A Review of Hypersonic Flow Separation and Control Characteristics. ASD-TDR-62-168, U.S. Air Force, Mar. 1962.

2. Kaufmann, Louis G., II; Meckler, Lawrence H.; Hartofilis, Stavros A.; and Weiss, Daniel: An Investigation of Hypersonic Flow Separation and Control Characteristics. AFFDL-TR-64-174, U.S. Air Force, Jan. 1965.

3. Wuerer, J. E.; and Clayton, F. I.: Flow Separation in High Speed Flight – A Review of the State-of-the-Art. Rept. SM-46429, Missile & Space Syst. Div., Douglas Aircraft Co., Apr. 1965.

4. Chapman, Dean R.; Kuehn, Donald M.; and Larson, Howard K.: Investigation of Separated Flows in Supersonic and Subsonic Streams With Emphasis on the Effect of Transition. NACA Rept. 1356, 1958.

5. Sterrett, James R.; and Emery, James C.: Extension of Boundary-Layer-Separation Criteria to a Mach Number of 6.5 by Utilizing Flat Plates With Forward-Facing Steps. NASA TN D-618, 1960.

6. Sterrett, James R.; and Emery, James C.: Experimental Separation Studies for Two-Dimensional Wedges and Curved Surfaces at Mach Numbers of 4.8 to 6.2. NASA TN D-1014, 1962.

7. Erdos, John; and Pallone, Adrian: Shock-Boundary Layer Interaction and Flow Separation. RAD-TR-61-23 (Contract AF04(647)-685), AVCO Corp., Aug. 15, 1961.

8. Bogdonoff, S. M.; and Vas, I. E.: Some Experiments on Hypersonic Separated Flows. ARC J., vol. 32, no. 10, Oct. 1962, pp. 1564-1572.

9. Miller, D. S.; Hijman, R.; and Childs, M. E.: Mach 8 to 22 Studies of Flow Separations Due to Deflected Control Surfaces. AIAA J., vol. 2, no. 2, Feb. 1964, pp. 312-321.

10. Sterrett, J. R.; and Holloway, P. F.: On the Effect of Transition on Parameters Within a Separation Region at Hypersonic Speeds – With Emphasis on Heat Transfer. Symposium on Fully Separated Flows, Arthur G. Hansen, ed., Amer. Soc. Mech. Eng., May 1964, pp. 15-26.

11. Gray, J. Don: A Correlation of Axisymmetric Laminar Flow Separation Characteristics. AIAA Paper No. 64-475, July 1964.

12. Kuehn, Donald M.: Laminar Boundary-Layer Separation Induced By Flares on Cylinders With Highly Cooled Boundary Layers at a Mach Number of 15. NASA TN D-2610, 1965.

13. Holloway, Paul F.; Sterrett, James R.; and Creekmore, Helen S.: An Investigation of Heat Transfer Within Regions of Separated Flow at a Mach Number of 6.0. NASA TN D-3074, 1965.

14. Townsend, James C.: Effects of Leading-Edge Bluntness and Ramp Deflection Angle on Laminar Boundary-Layer Separation In Hypersonic Flow. NASA TN D-3290, 1966.

15. Needham, David A.; and Stollery, John L.: Boundary Layer Separation In Hypersonic Flow. AIAA Paper No. 66-455, June 1966.

16. Giles, H. L.: and Thomas, J. W.: Analysis of Hypersonic Pressure and Heat Transfer Tests on a Flat Plate With a Flap and a Delta Wing With Body, Elevons, Fins, and Rudders. NASA CR-536, 1966.

17. Holden, Michael S.: Experimental Studies of Separated Flows at Hypersonic Speeds. Part II: Two-Dimensional Wedge Separated Flow Studies. AIAA J., vol. 4, no. 5, May 1966, pp. 790-799.

18. Popinski, Z.; and Ehrlich, C. F.: Development Design Methods for Predicting Hypersonic Aerodynamic Control Characteristics. AFFDL-TR-66-85, U.S. Air Force, Sept. 1966. (Available from DDC as AD 644251.)

19. Lees, Lester; and Reeves, Barry L.: Supersonic Separated and Reattaching Laminar Flows. I. General Theory and Application to Adiabatic Boundary-Layer/Shock-Wave Interactions. AIAA J., vol. 2, no. 11, Nov. 1964, pp. 1907-1920.

20. Johnson, Charles Borden: A Theoretical and Experimental Study at Mach 8 of Flow Separation of a Flat Plate With Deflected Trailing Edge Flap. M.S. Thesis, Virginia Polytech. Inst., 1966.

21. Nielsen, Jack N.; Lynes, Larry L.; and Goodwin, Frederick K.: Calculation of Laminar Separation With Free Interaction by the Method of Integral Relations. Part I – Two-Dimensional Supersonic Adiabatic Flow. AFFDL-TR-65-107, U.S. Air Force, Oct. 1965. (Available from DDC as AD 626160.)

22. Nielsen, Jack N.; Lynes, Larry L.; and Goodwin, Frederick K.: Calculation of Laminar Separation With Free Interaction by the Method of Integral Relations. Part II – Two-Dimensional Supersonic Nonadiabatic Flow and Axisymmetric Supersonic Adiabatic and Nonadiabatic Flows. AFFDL-TR-65-107, U.S. Air Force, Jan. 1966. (Available from DDC as AD 630765.)

23. Holden, M. S.: An Analytical Study of Separated Flows Induced by Shock Wave – Boundary Layer Interaction. NASA CR-600, 1966.

24. Putnam, Lawrence E.: Investigation of Effects of Ramp Span and Deflection Angle on Laminar Boundary-Layer Separation at Mach 10.03. NASA TN D-2833, 1965.

25. Crawford, Davis H.: The Effect of Air Bleed on the Heat Transfer and Pressure Distribution on 30° Conical Flares at a Mach Number of 6.8. NASA TM X-439, 1961.

26. Stern, I.; and Rowe, W. H., Jr.: Effect of Gap Size on Pressure and Heating Over the Flap of a Blunt Delta Wing in Hypersonic Flow. J. Spacecraft Rockets, vol. 4, no. 1, Jan. 1967, pp. 109-114.

27. Dunavant, James C.; and Stone, Howard W.: Effect of Roughness on Heat Transfer to Hemisphere Cylinders at Mach Numbers 10.4 and 11.4. NASA TN D-3871, 1967.

28. Erickson, Wayne D.; and Creekmore, Helen S.: A Study of Equilibrium Real-Gas Effects in Hypersonic Air Nozzles, Including Charts of Thermodynamic Properties for Equilibrium Air. NASA TN D-231, 1960.

29. Lucks, C. F.; and Deem, H. W.: Thermal Properties of Thirteen Metals. Spec. Tech. Publ. No. 227, Amer. Soc. Testing Mater., 1958.

30. Dennard, John S.; and Spencer, Patricia B.: Ideal-Gas Tables for Oblique-Shock Flow Parameters in Air at Mach Numbers From 1.05 to 12.0. NASA TN D-2221, 1964.

31. Bertram, Mitchel H.: Hypersonic Laminar Viscous Interaction Effects on the Aerodynamics of Two-Dimensional Wedge and Triangular Planform Wings. NASA TN D-3523, 1966.

32. Bertram, M. H.; Weinstein, L. M.; Cary, A. M., Jr.; and Arrington, J. P.: Effect of Two-Dimensional Multiple-Wave Distortions on the Heat Transfer to a Wall in Hypersonic Flow. AIAA Paper no. 67-164, Jan. 1967.

33. Cooke, J. C.: Separated Supersonic Flow. Tech. Note No. Aero. 2879, Brit. R.A.E., Mar. 1963.

34. Becker, John V.; and Korycinski, Peter F.: Heat Transfer and Pressure Distribution at a Mach Number of 6.8 on Bodies With Conical Flares and Extensive Flow Separation. NASA TN D-1260, 1962.

35. Needham, D. A.; and Stollery, J. L.: Hypersonic Studies of Incipient Separation and Separated Flows. Separated Flows, Pt. 1, AGARD CP No. 4, May 1966, pp. 89-119.

36. Monaghan, R. J.: An Approximate Solution of the Compressible Laminar Boundary Layer on a Flat Plate. R. & M. No. 2760, Brit. A.R.C., 1953.

37. Spalding, D. B.; and Chi, S. W.: The Drag of a Compressible Turbulent Boundary Layer on a Smooth Flat Plate With and Without Heat Transfer. J. Fluid Mech., vol. 18, pt. 1, Jan. 1964, pp. 117-143.

38. Bertram, Mitchel H.; and Neal, Luther, Jr.: Recent Experiments in Hypersonic Turbulent Boundary Layers. Presented to the AGARD Specialists Meeting on Recent Developments in Boundary-Layer Research (Naples, Italy), May 10-14, 1965.

39. Neal, Luther, Jr.; and Bertram, Mitchel H.: Turbulent-Skin-Friction and Heat-Transfer Charts Adapted From the Spalding and Chi Method. NASA TN D-3969, 1967.

TABLE I.- LOCATION OF INSTRUMENTATION

Thermocouple	x		y	
	inch	cm	inch	cm
1	11.69	29.69	1.00	2.54
2	12.70	32.26	-1.00	-2.54
3	13.70	34.80	1.00	2.54
4	15.82	40.18	-1.00	-2.54
5	16.83	42.75	1.00	2.54
6	17.84	45.31	-1.00	-2.54
7	18.10	45.97	1.00	2.54
*8	19.90	50.55	1.00	2.54
*9	21.00	53.34	-1.00	-2.54
*10	21.63	54.94	1.00	2.54
*11	21.88	55.57	-1.00	-2.54
*12	22.12	56.18	1.00	2.54
*13	22.37	56.82	-1.00	-2.54
*14	22.62	57.45	1.00	2.54
*15	22.87	58.09	-1.00	-2.54
16	23.71	60.22	1.00	2.54
17	23.96	60.86	-1.00	-2.54
18	24.21	61.49	1.00	2.54
19	24.46	62.13	-1.00	-2.54
20	24.71	62.76	1.00	2.54
21	24.96	63.40	-1.00	-2.54
22	25.46	64.67	1.00	2.54
23	25.96	65.94	-1.00	-2.54
24	26.46	67.21	1.00	2.54
25	26.96	68.48	-1.00	-2.54
26	27.46	69.75	1.00	2.54
27	27.96	71.02	-1.00	-2.54
28	28.46	72.29	1.00	2.54
29	28.96	73.56	-1.00	-2.54
30	29.46	74.83	1.00	2.54

Pressure orifice	x		Instrument (range)
	inch	cm	
1	11.69	29.69	Ionization gage
2	13.70	34.80	Transducer (0 to 1 psia)
3	15.82	40.18	Ionization gage
4	17.84	45.31	Transducer (0 to 1 psia)
*5	19.90	50.55	Ionization gage
*6	21.63	54.94	Transducer (0 to 1 psia)
*7	22.12	56.18	Transducer (0 to 3 psia)
*8	22.62	57.45	Transducer (0 to 3 psia)
9	23.71	60.22	Transducer (0 to 3 psia)
10	24.21	61.49	Transducer (0 to 10 psia)
11	24.71	62.76	Transducer (0 to 15 psia)
12	25.46	64.67	Transducer (0 to 15 psia)
13	26.46	67.21	Transducer (0 to 15 psia)
14	27.46	69.75	Transducer (0 to 3 psia)
15	28.46	72.79	Transducer (0 to 15 psia)
16	29.46	74.83	Transducer (0 to 10 psia)

*The locations of x vary slightly with gap size. The locations listed are for $\epsilon/r_1 = 0.208$.

TABLE II.- TEST PROGRAM

α, deg	δ_f, deg	ϵ/r_1	Gap entrance
p_t = 300 lb/sq in. abs $(20.7 \times 10^5$ N/m$^2)$			
6.83	0	Sealed	Sharp
↓	10	↓	↓
↓	20	↓	↓
↓	0	0.520	Sharp
↓	10	↓	↓
↓	20	↓	↓
↓	0	.208	Sharp
↓	10	↓	↓
↓	20	↓	↓
p_t = 1500 lb/sq in. abs $(103.5 \times 10^5$ N/m$^2)$			
6.83	0	Sealed	Sharp
↓	10	↓	↓
↓	20	↓	↓
↓	30	↓	↓
↓	0	0.052	Sharp and rounded
↓	10	↓	↓
↓	20	↓	↓
↓	30	↓	↓
↓	0	.104	Sharp
↓	10	↓	↓
↓	20	↓	↓
↓	30	↓	↓
↓	0	.208	Sharp and rounded
↓	10	↓	↓
↓	20	↓	↓
↓	30	↓	↓
↓	0	.416	Rounded
↓	10	↓	↓
↓	20	↓	↓
↓	30	↓	↓
12.83	0	.052	Sharp and rounded
↓	10	↓	↓
↓	20	↓	↓
↓	0	.208	Sharp and rounded
↓	10	↓	↓
↓	20	↓	↓

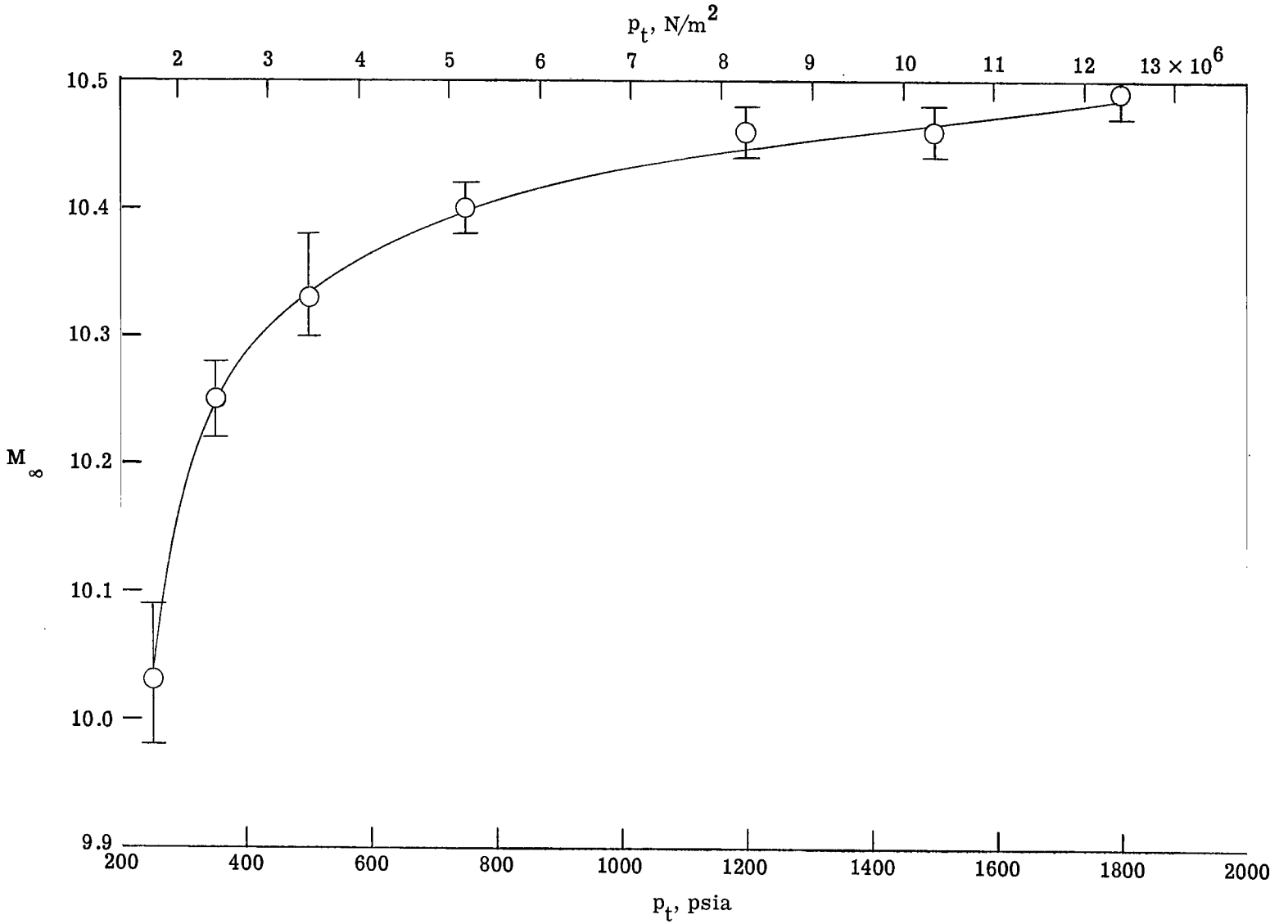

Figure 1.- Mach number calibration of Langley continuous-flow hypersonic tunnel with beryllium-copper throat.

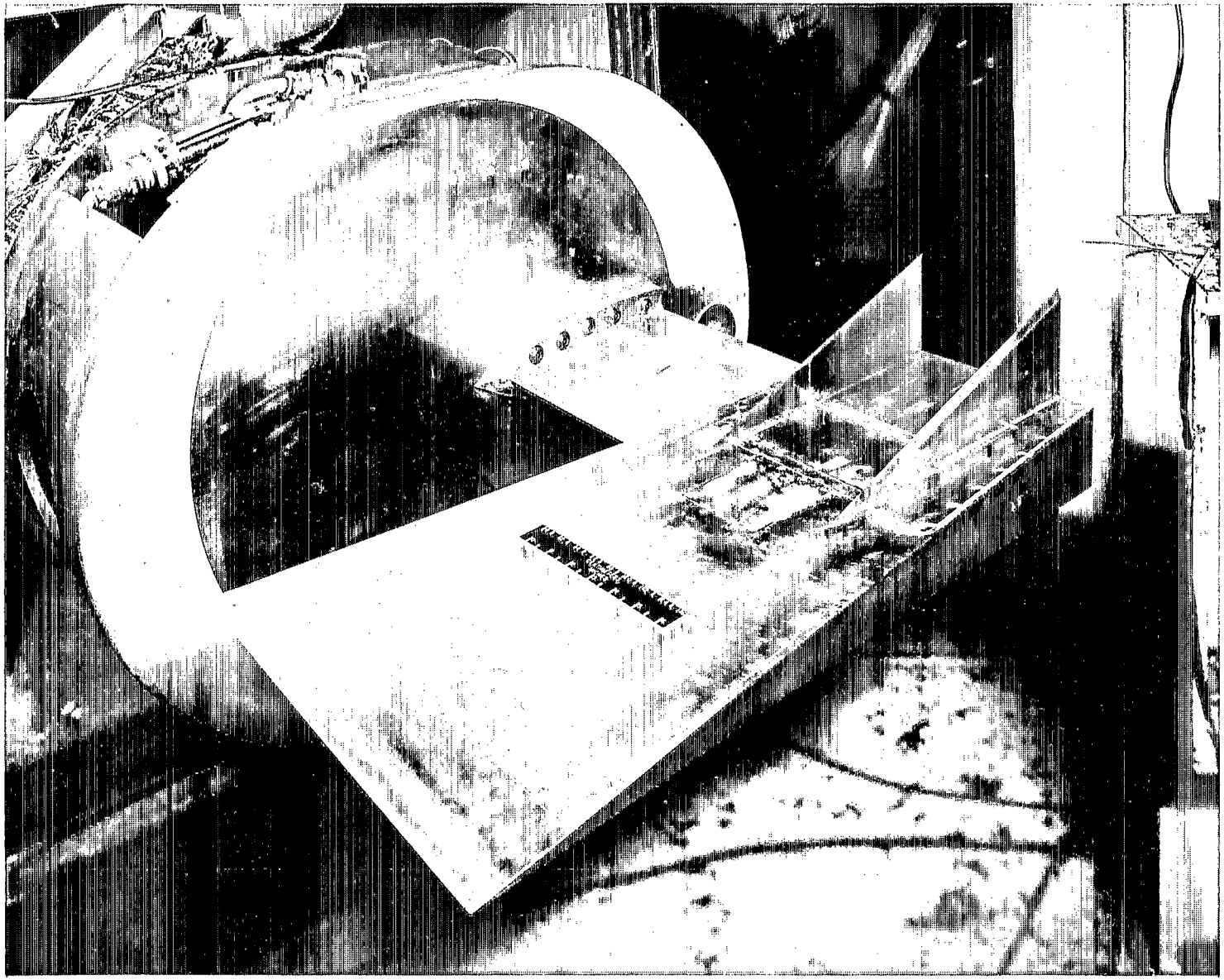

Figure 2.- Photograph of model.

L-66-5932

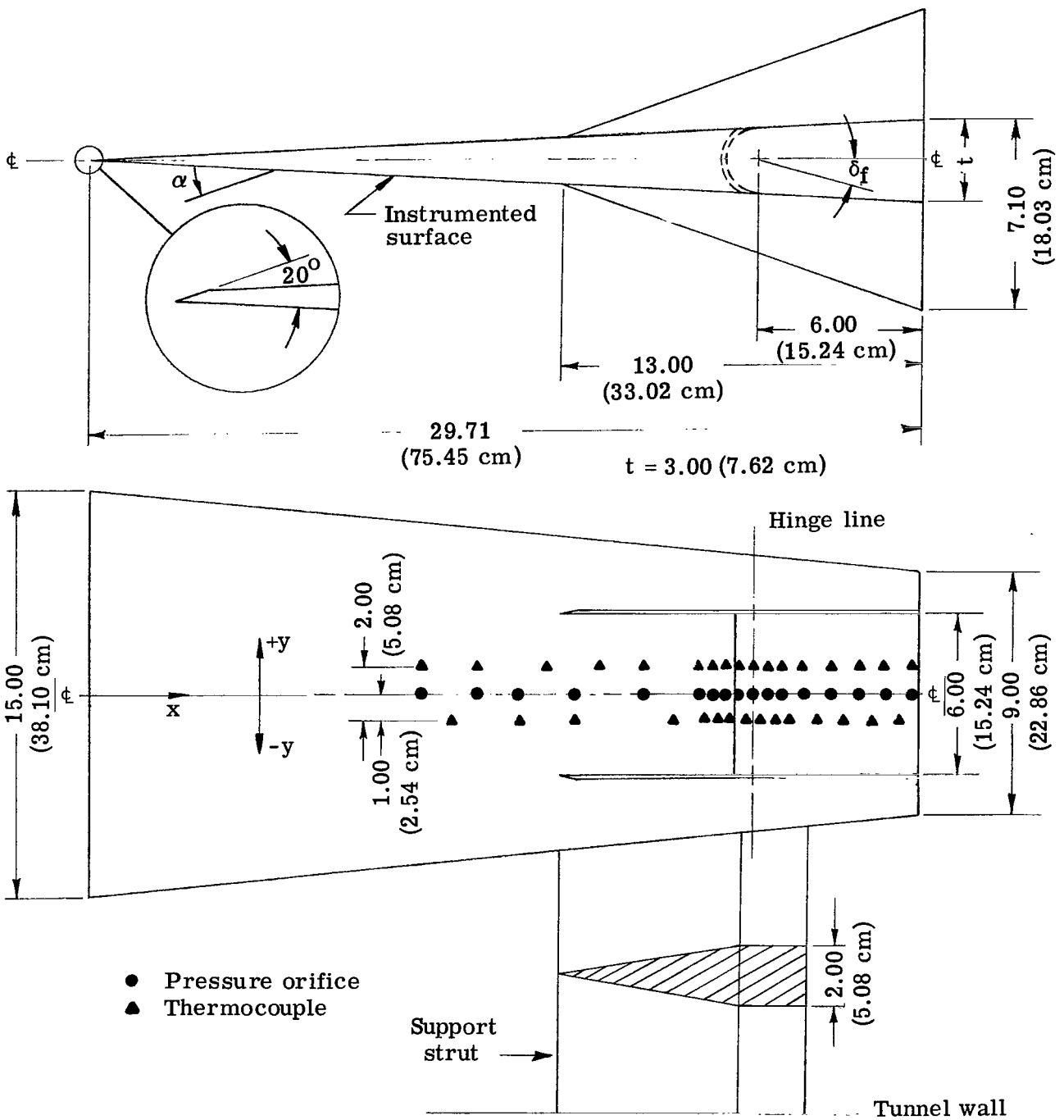

(a) Basic configuration.

Figure 3.- Sketch of model. Dimensions are in inches (centimeters).

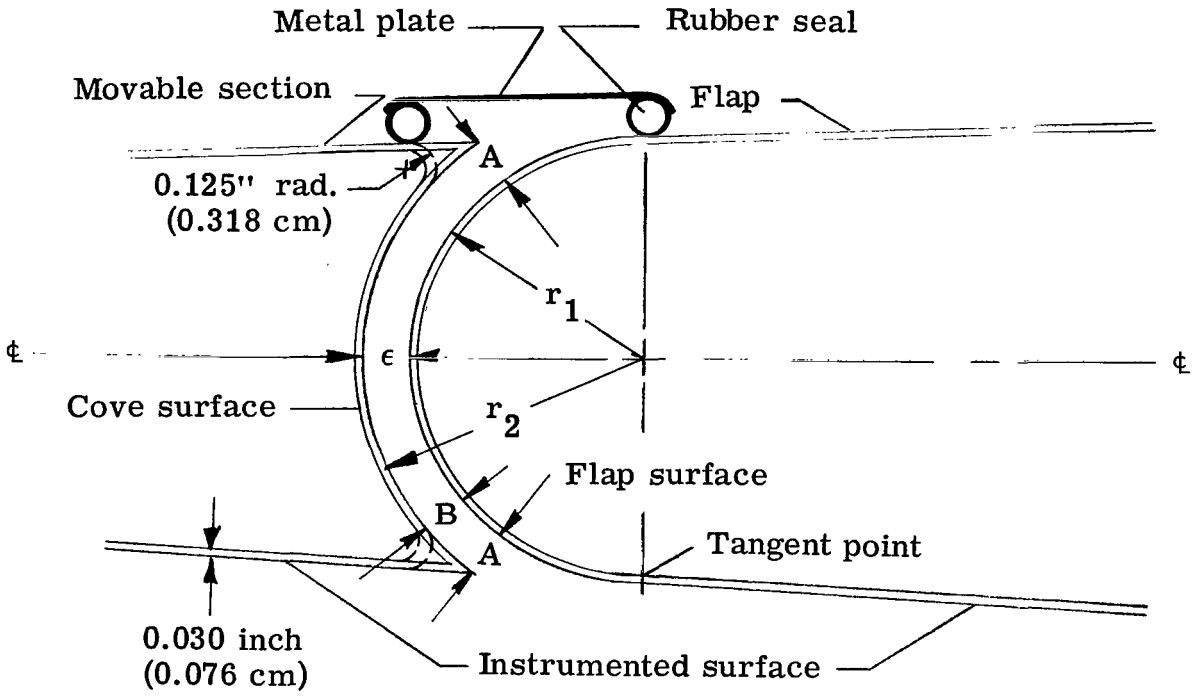

			Sharp lip		Radiused lip	
$\frac{\epsilon}{r_1}$	ϵ		A		B	
	inch	cm	inch	cm	inch	cm
0.0520	0.0625	0.1588	0.150	0.381	0.110	0.279
.1040	.1250	.3175	.175	.445	—	—
.2080	.2500	.6350	.250	.635	.250	.635
.4160	.500	1.2700	—	—	.450	1.143

r_1 = 1.202 in. (3.053 cm)

r_2 = 1.450 in. (3.683 cm)

(b) Details of gap.

Figure 3.- Concluded.

Figure 4.- Photograph of distorted flap surface. L-67-2002

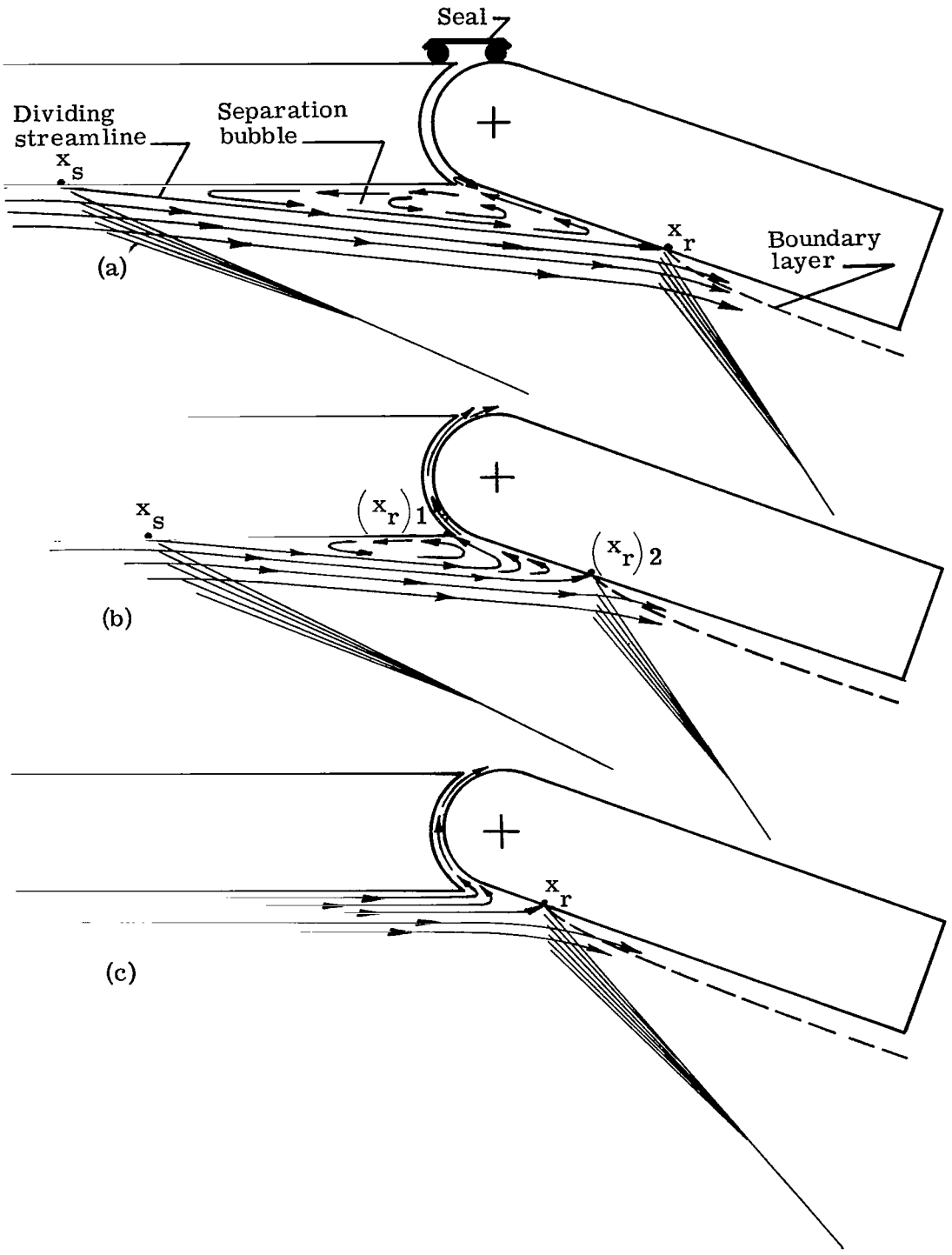

Figure 5.- Flow model.

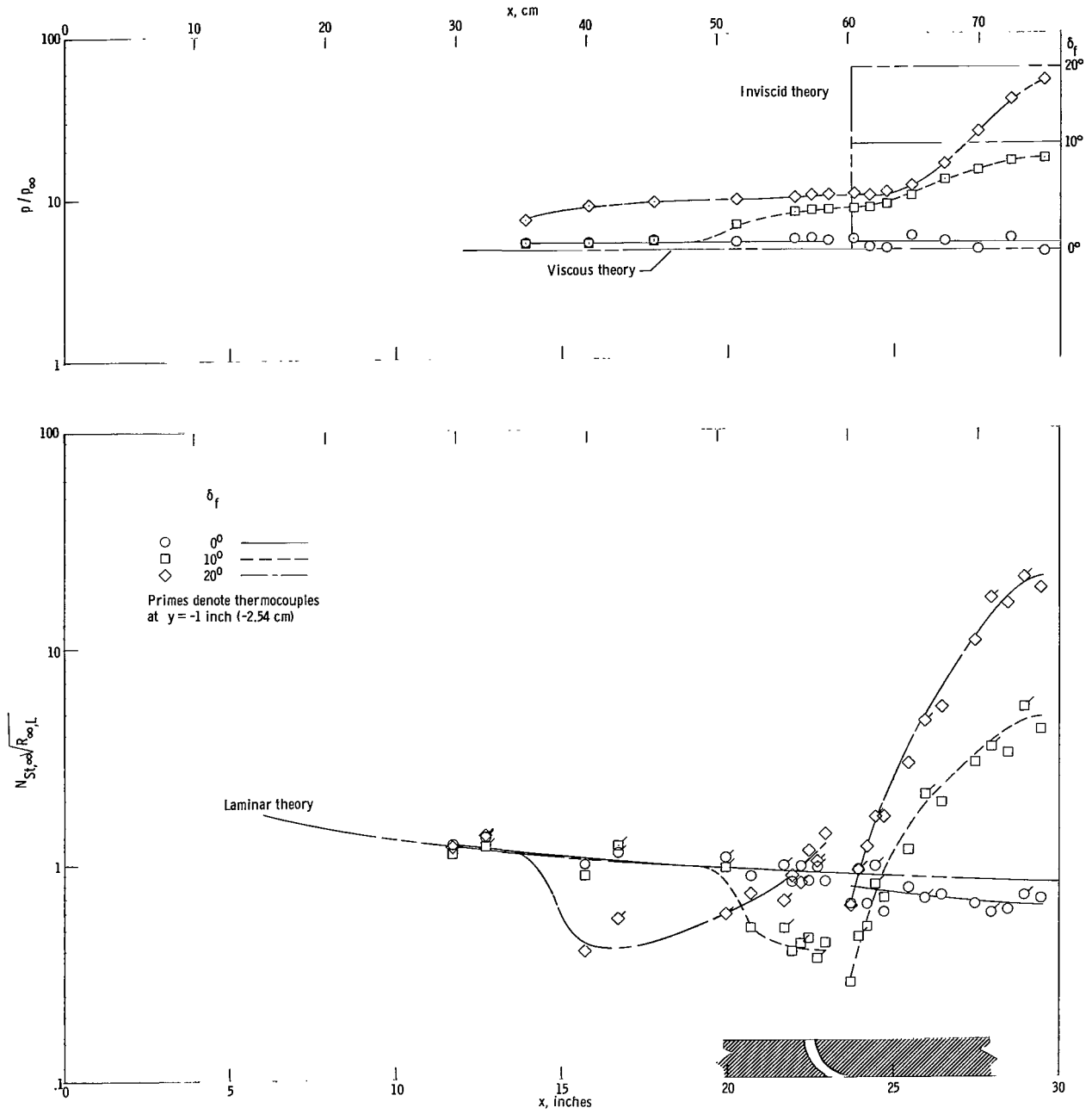

(a) Sealed gap.

Figure 6.- Effect of gap size and flap deflection on pressure and heat-transfer distributions for sharp lip configurations at $R_{\infty,L} = 0.8 \times 10^6$, $\alpha = 6.83^0$.

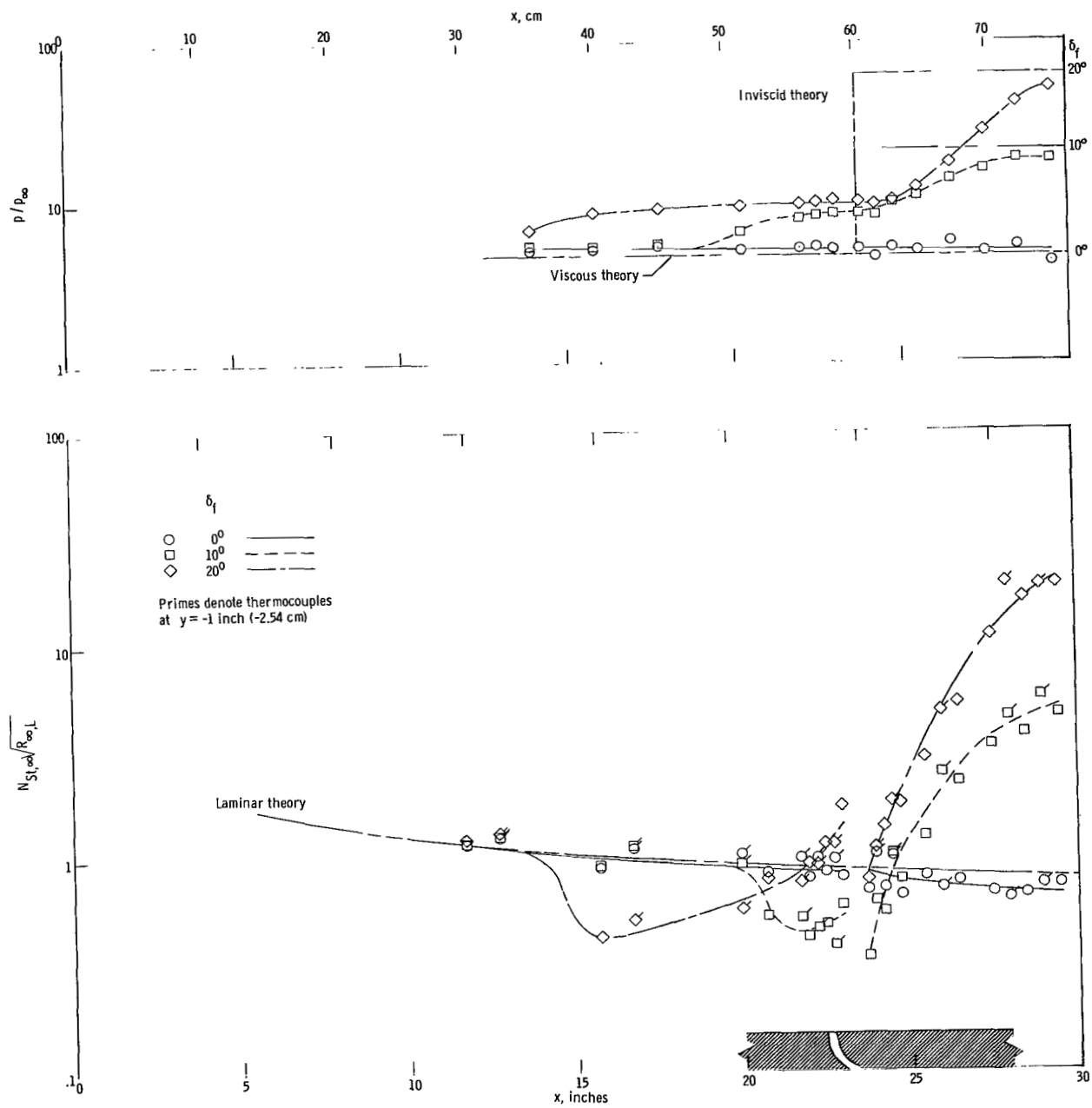

(b) $\varepsilon/r_1 = 0.052$.

Figure 6.- Continued.

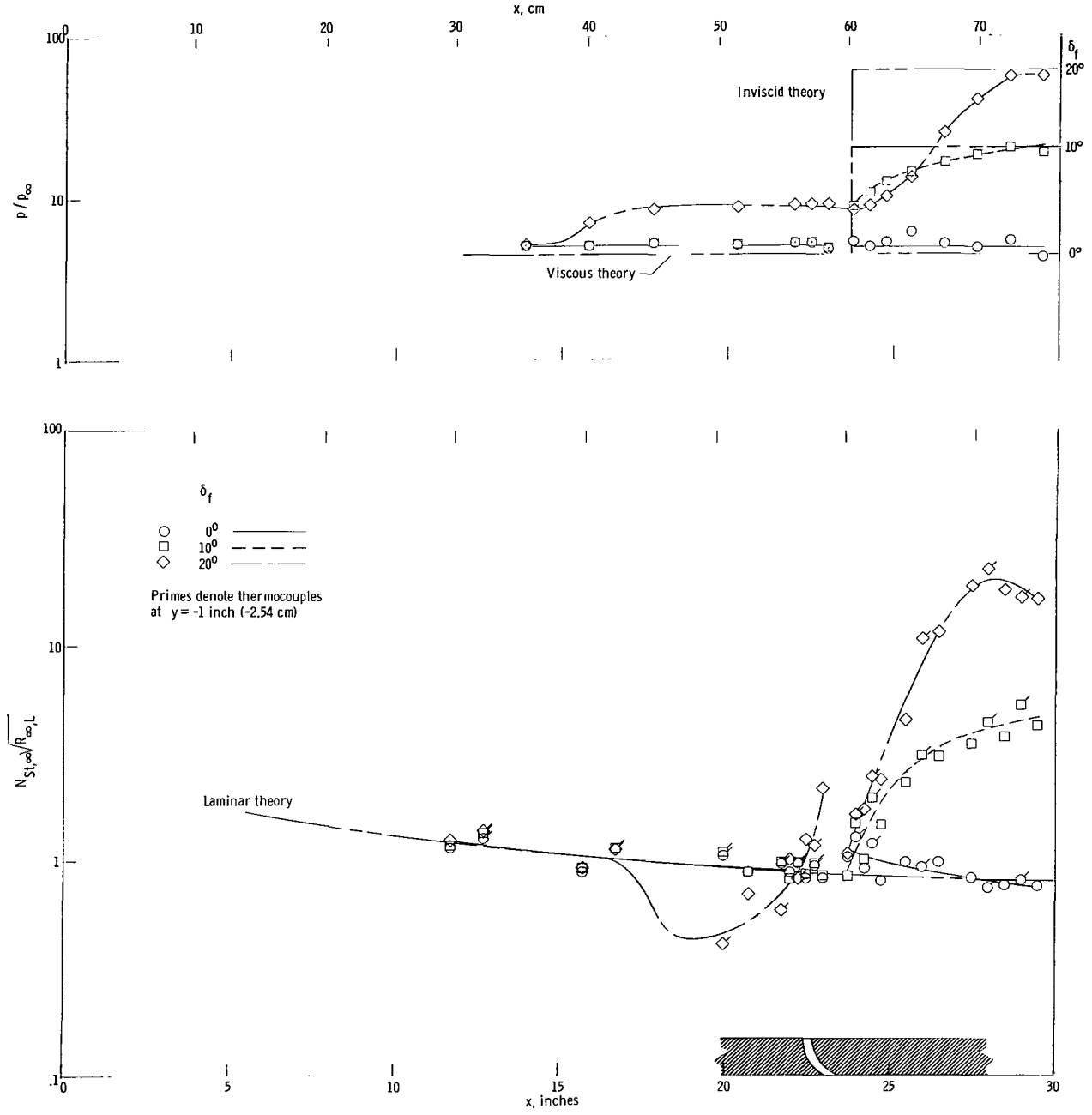

(c) $\epsilon/r_1 = 0.208$.

Figure 6.- Concluded.

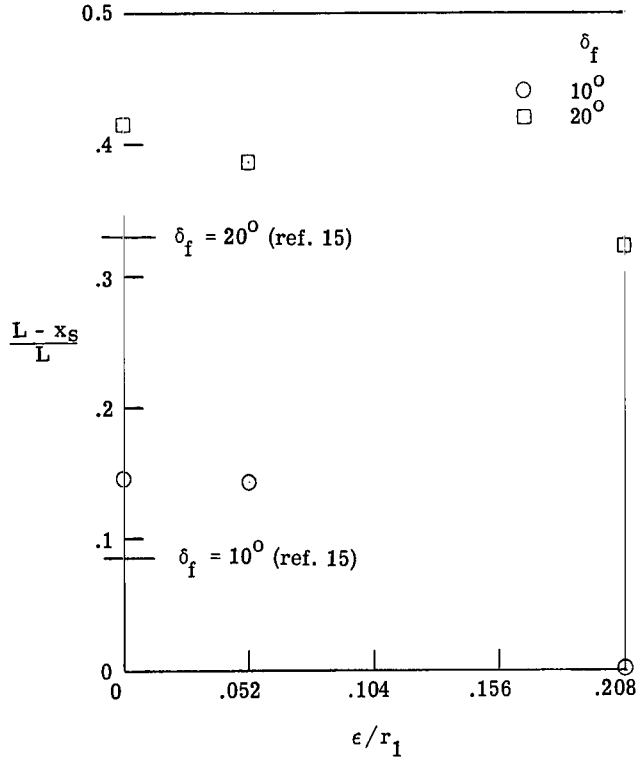

Figure 7.- Effect of gap size and flap deflection on length of laminar separation for $R_{\infty,L} \approx 0.8 \times 10^6$, $\alpha = 6.83^o$.

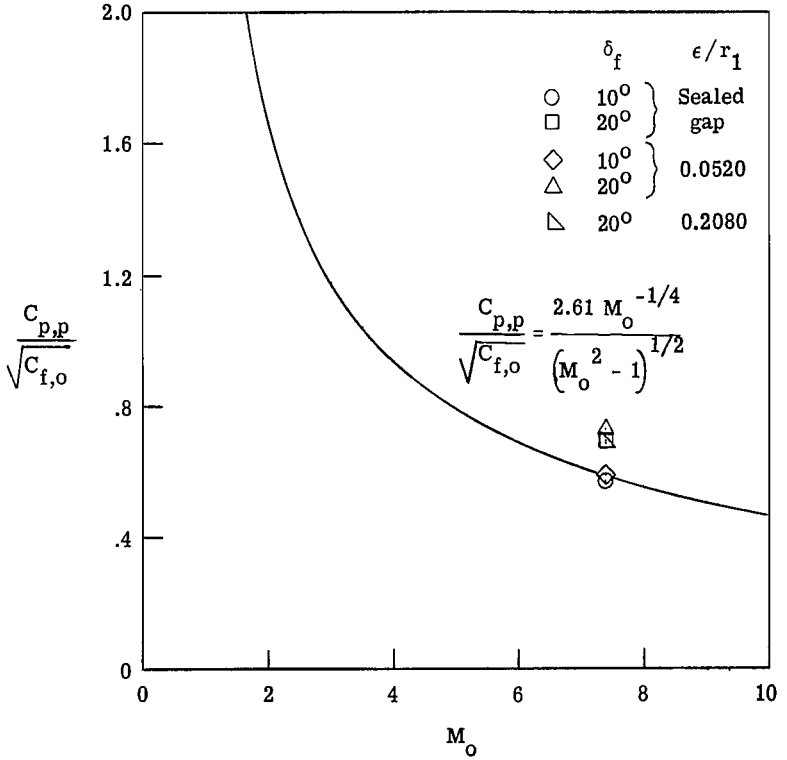

Figure 8.- Correlation of laminar plateau pressure coefficients for $R_{\infty,L} \approx 0.8 \times 10^6$, $\alpha = 6.83^o$.

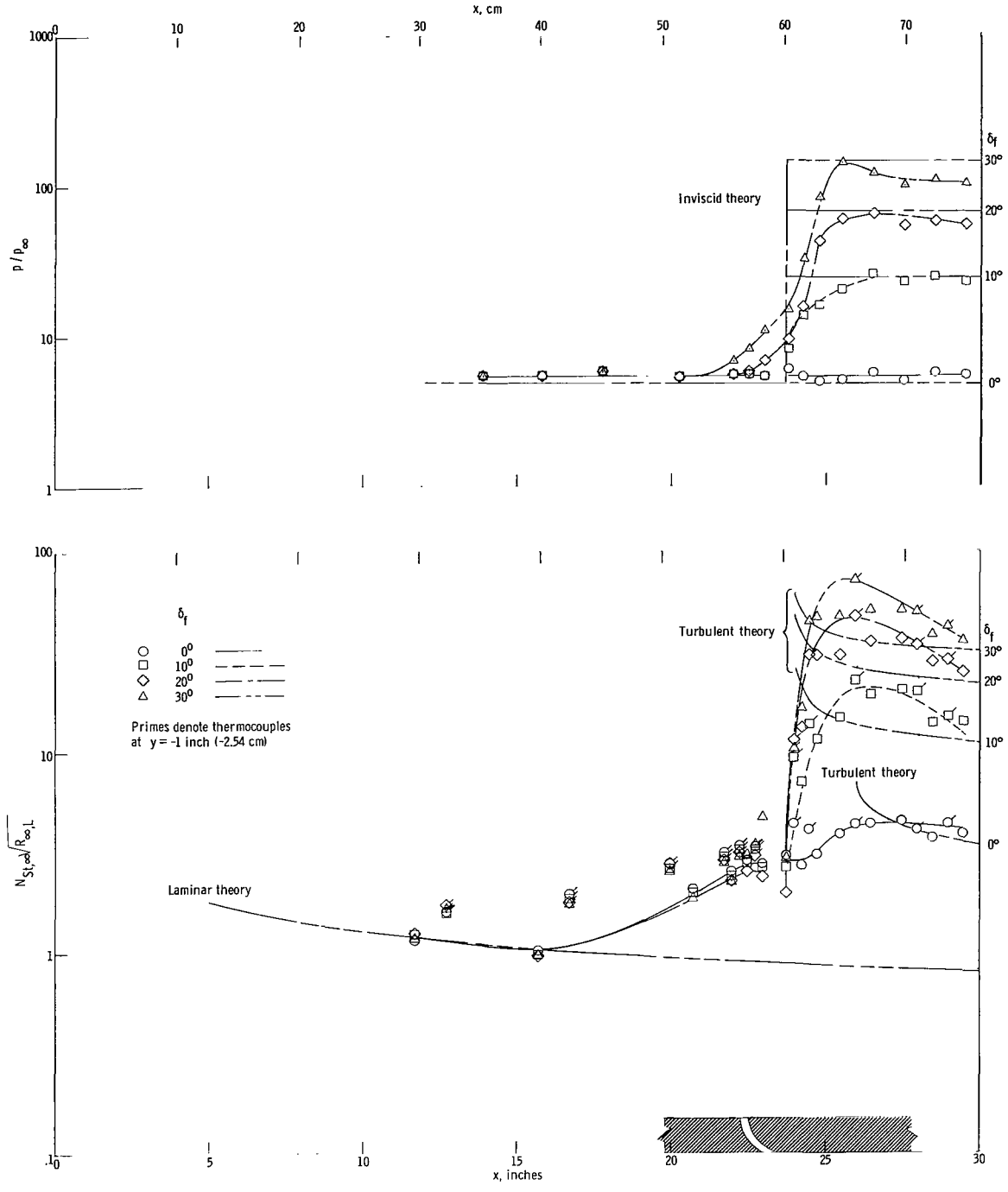

(a) Sealed gap.

Figure 9.- Effect of gap size and flap deflection on pressure and heat-transfer distributions for sharp lip configurations at $R_{\infty,L} = 3.6 \times 10^6$, $\alpha = 6.83^0$.

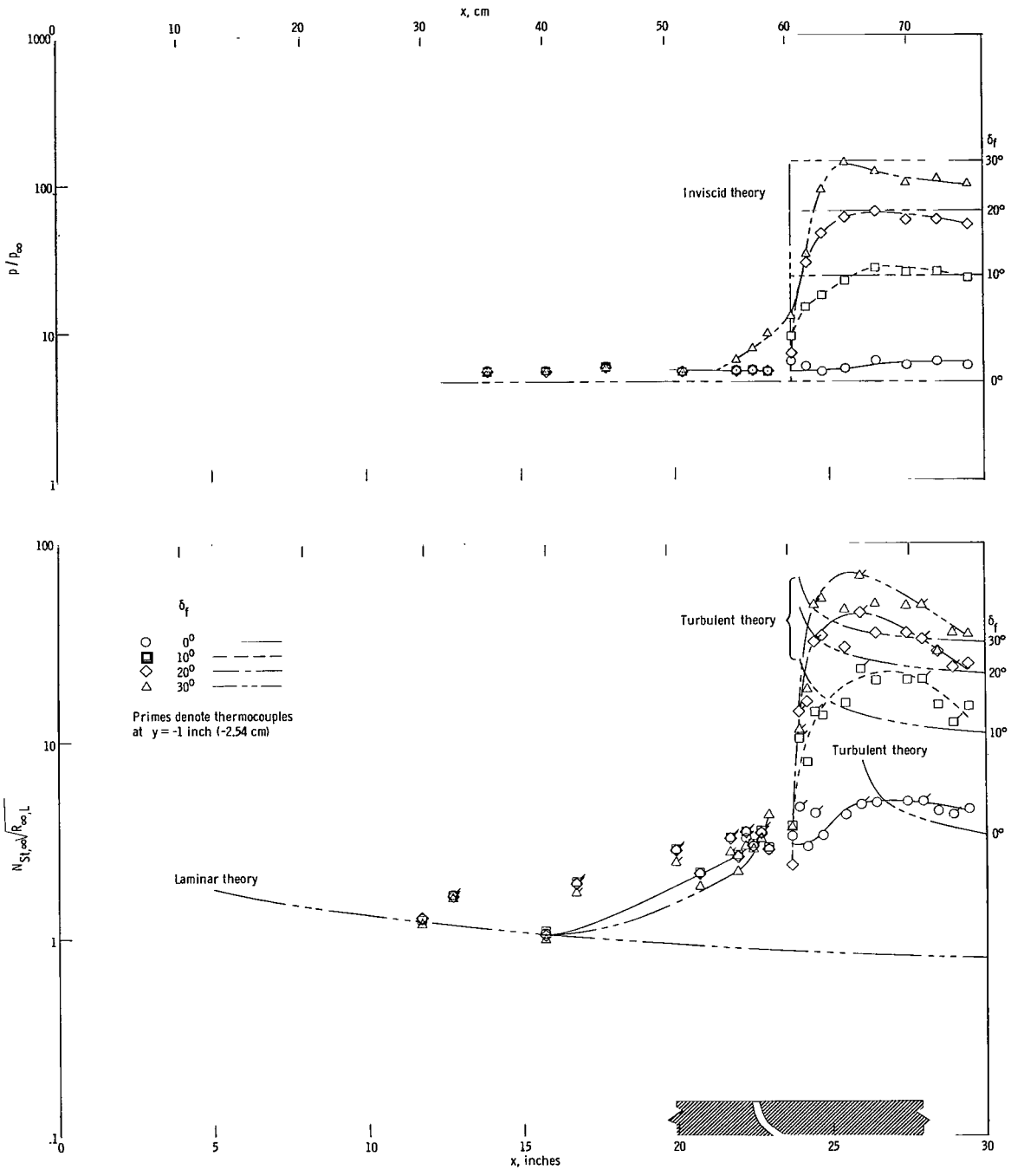

(b) $\varepsilon/r_1 = 0.052$.

Figure 9.- Continued.

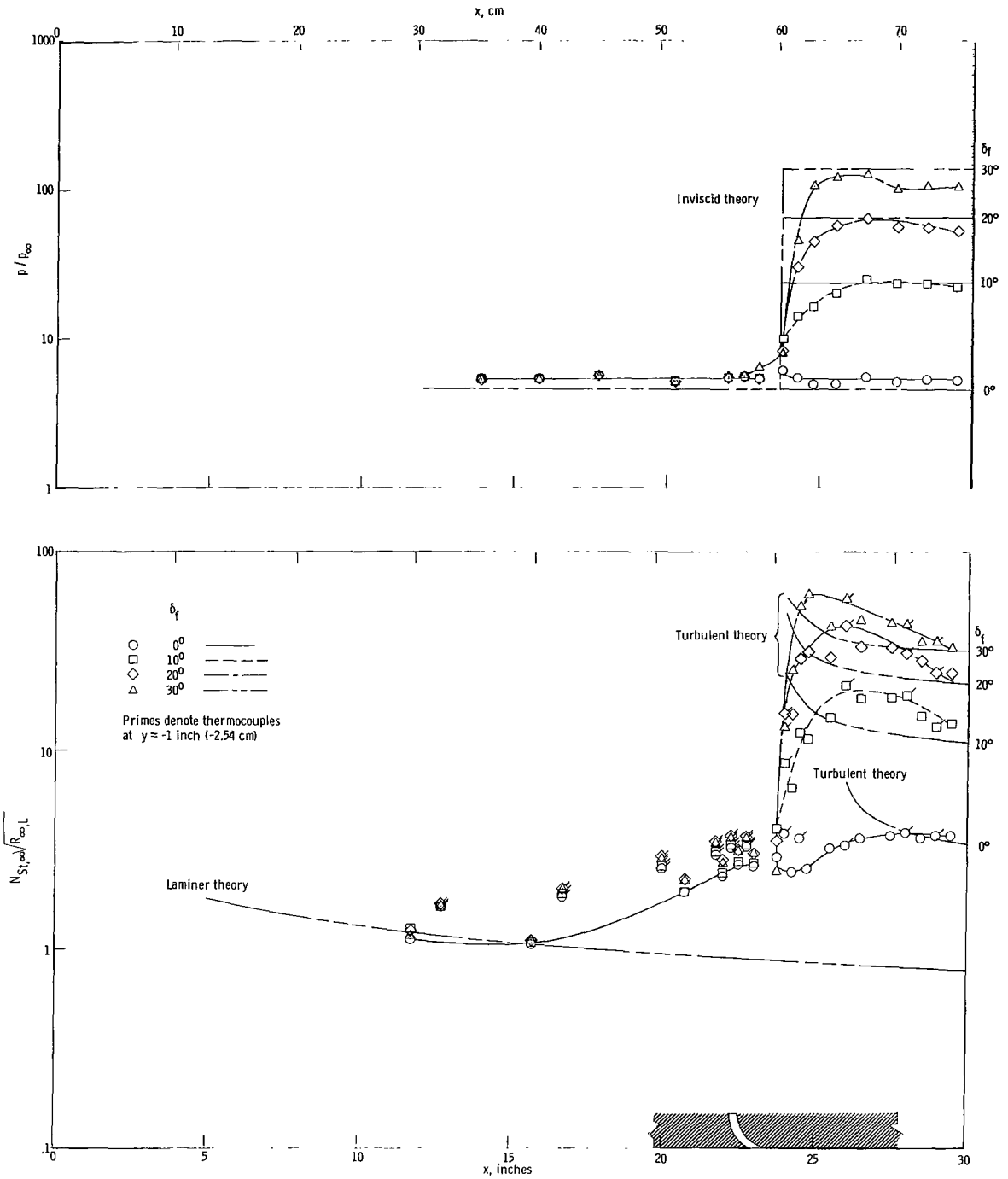

(c) $\varepsilon/r_1 = 0.104$.

Figure 9.- Continued.

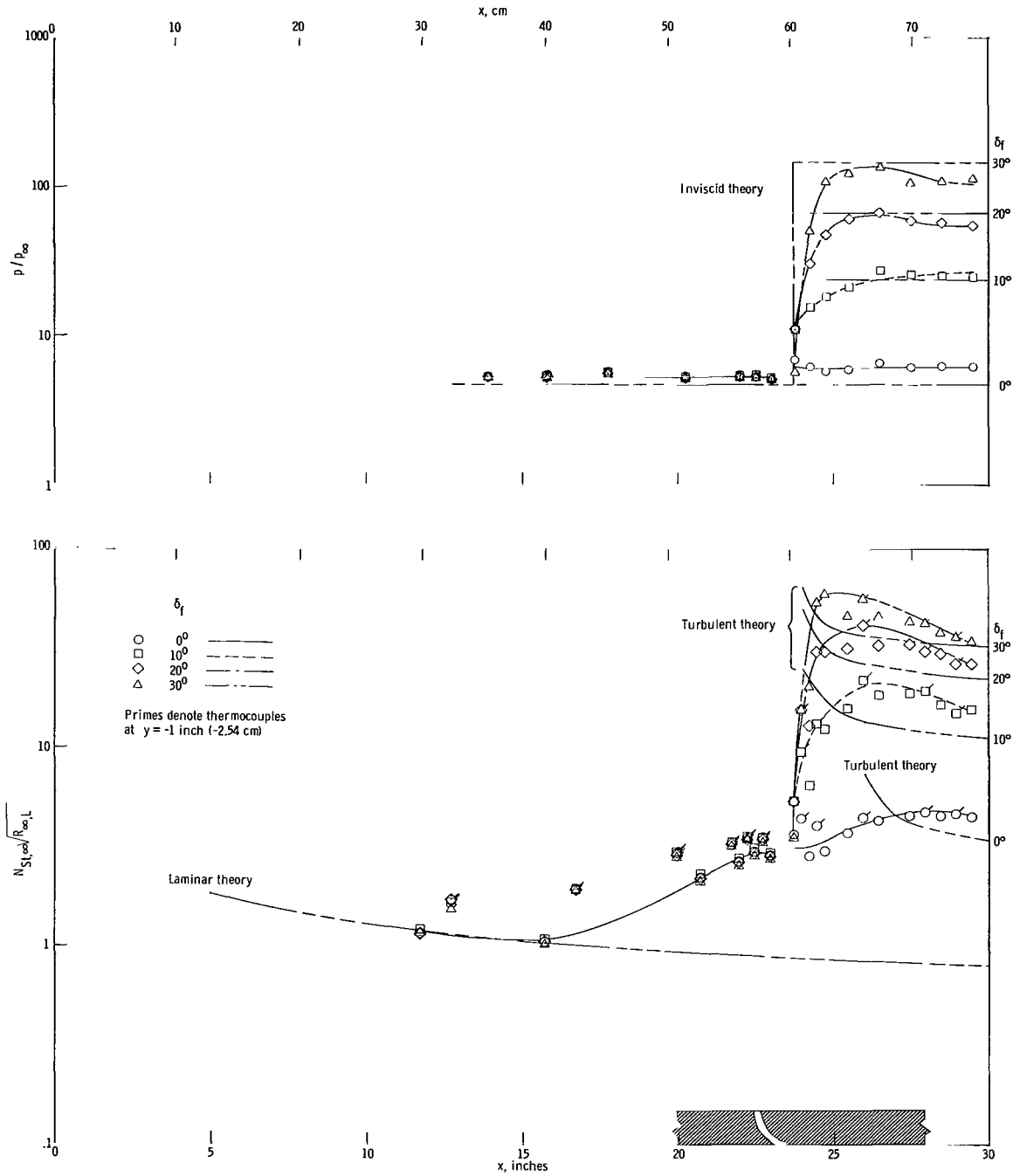

(d) $\varepsilon/r_1 = 0.208$.

Figure 9.- Concluded.

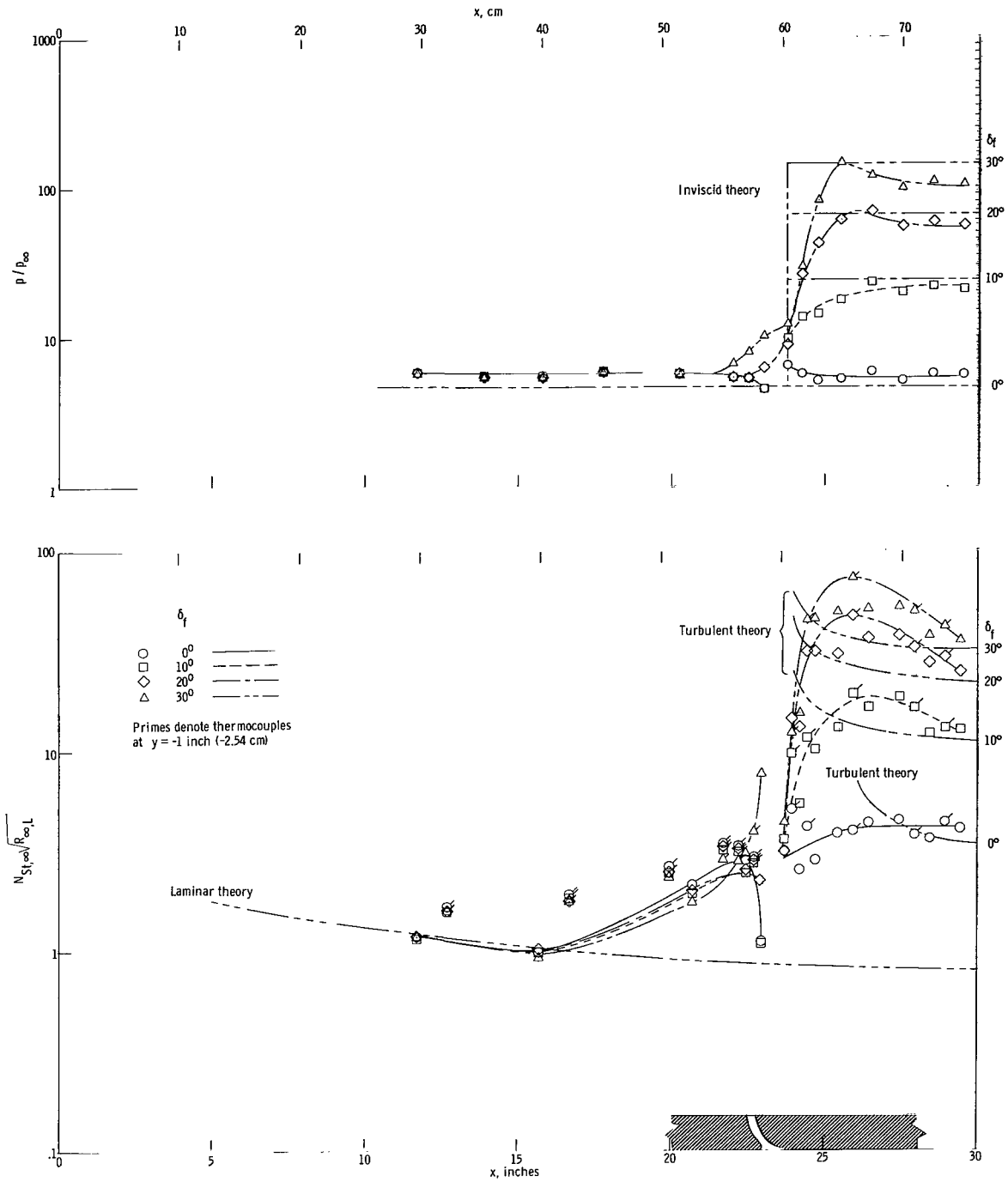

(a) $\varepsilon/r_1 = 0.052$.

Figure 10.- Effect of gap size and flap deflection on pressure and heat-transfer distributions with rounded lip at $R_{\infty,L} = 3.6 \times 10^6$, $\alpha = 6.83^0$.

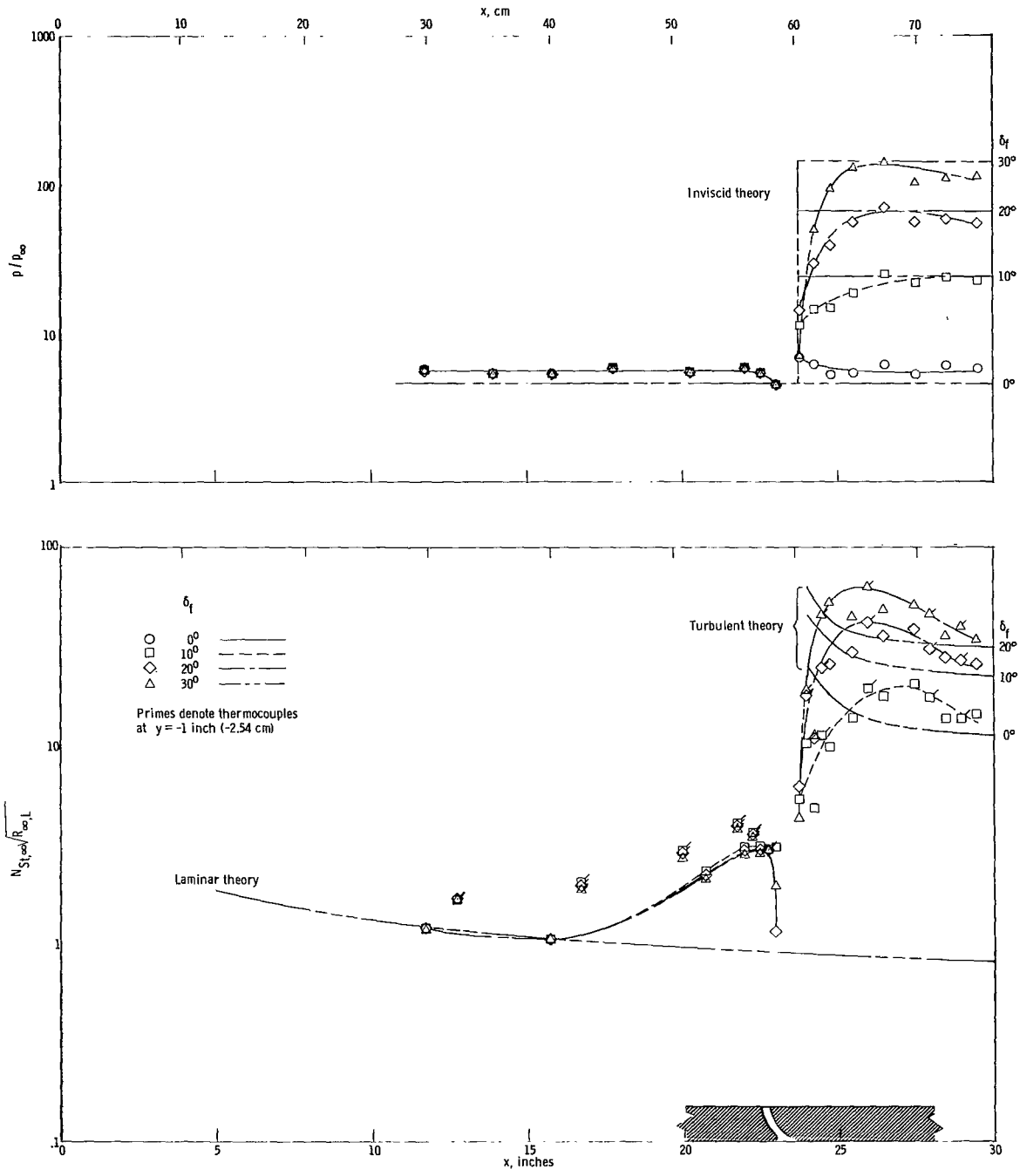

(b) $\varepsilon/r_1 = 0.208$.

Figure 10.- Continued.

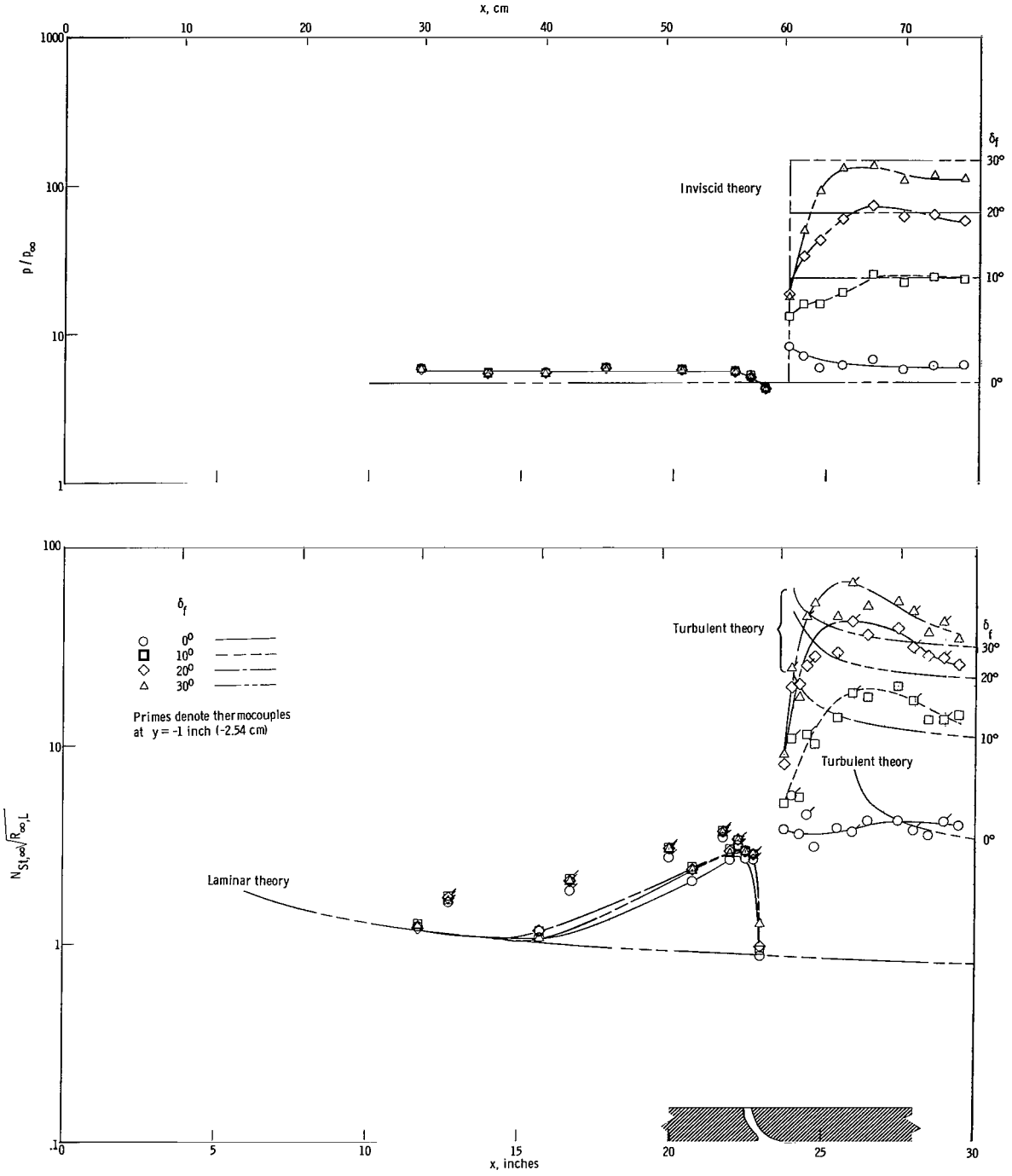

(c) $\varepsilon/r_1 = 0.416$.

Figure 10.- Concluded.

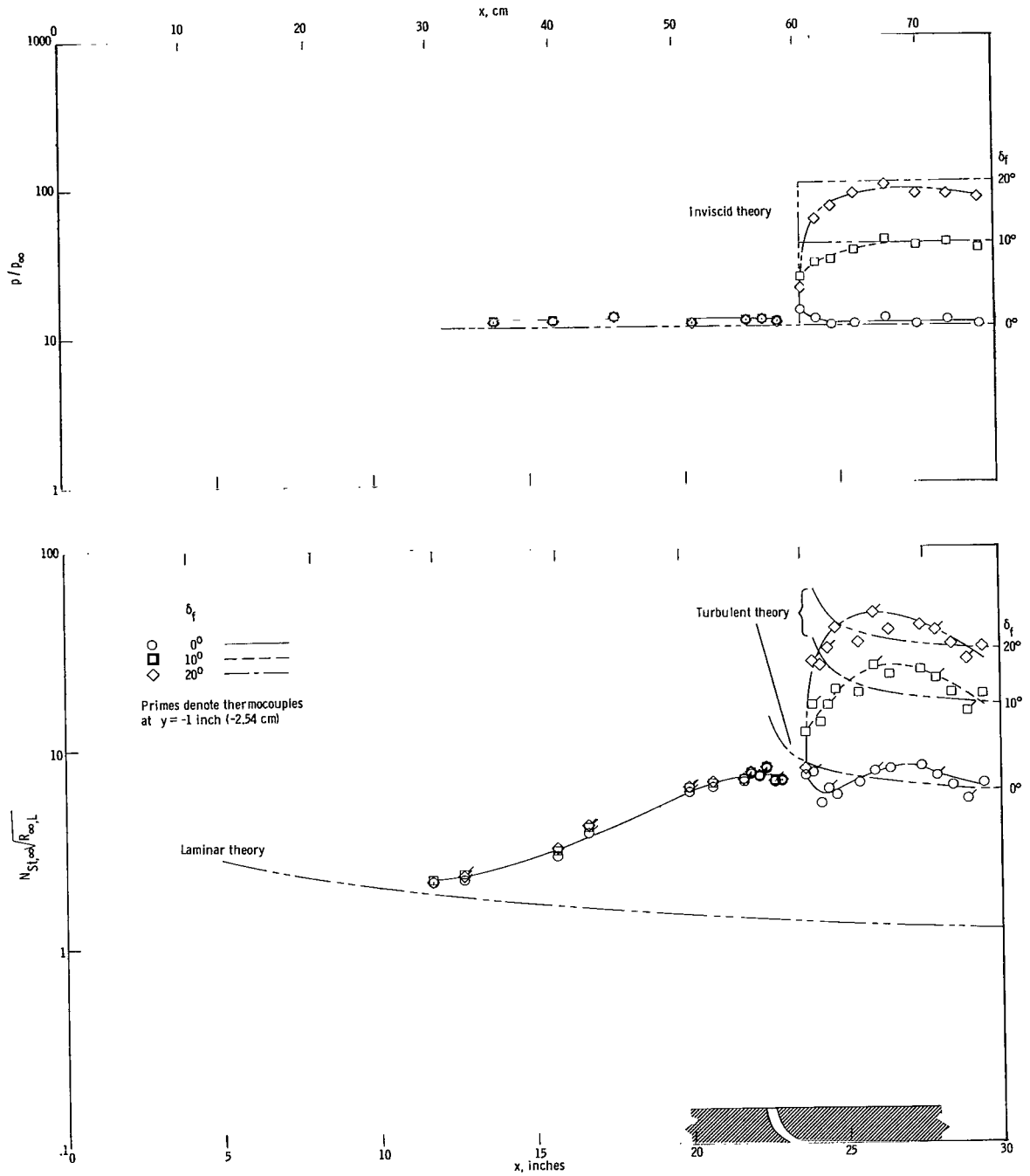

(a) $\varepsilon/r_1 = 0.052$.

Figure 11.- Effect of gap size and flap deflection on pressure and heat-transfer distributions with a sharp lip at $R_{\infty,L} = 3.6 \times 10^6$, $\alpha = 12.83^0$.

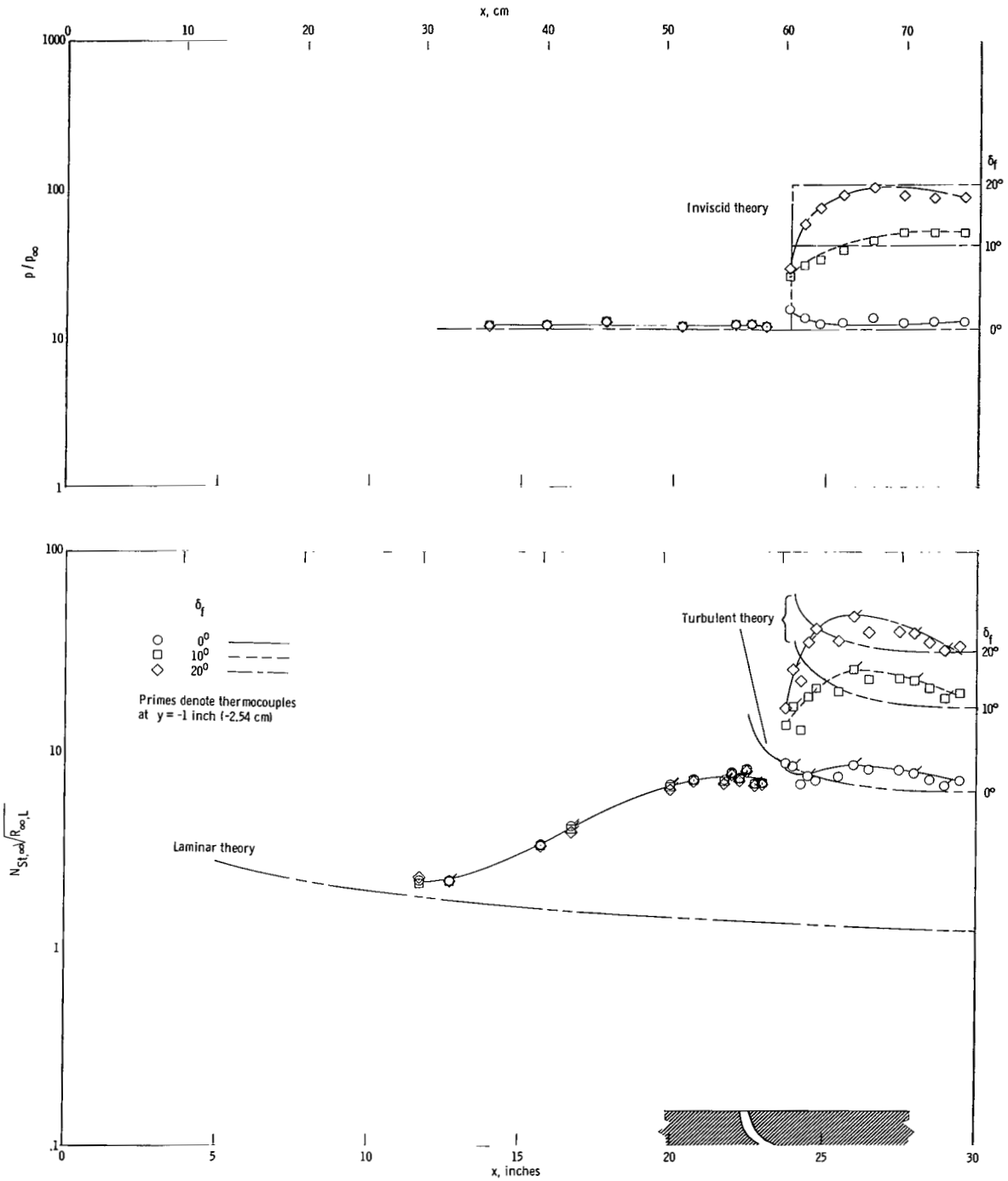

(b) $\varepsilon/r_1 = 0.208$.

Figure 11.- Concluded.

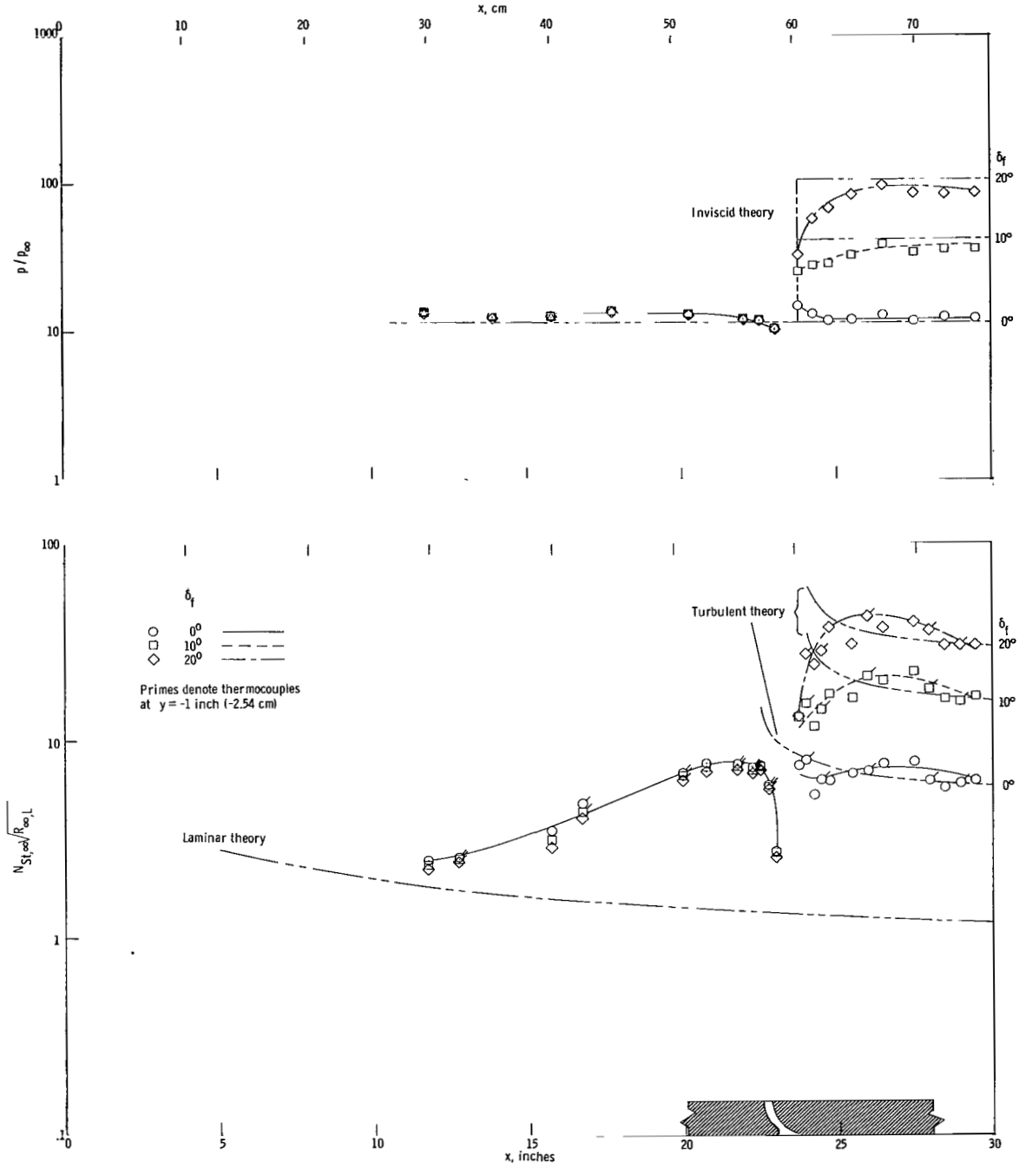

(a) $\varepsilon/r_1 = 0.052$.

Figure 12.- Effect of gap size and flap deflection on pressure and heat-transfer distributions with rounded lip at $R_{\infty,L} = 3.6 \times 10^6$, $\alpha = 12.83^0$.

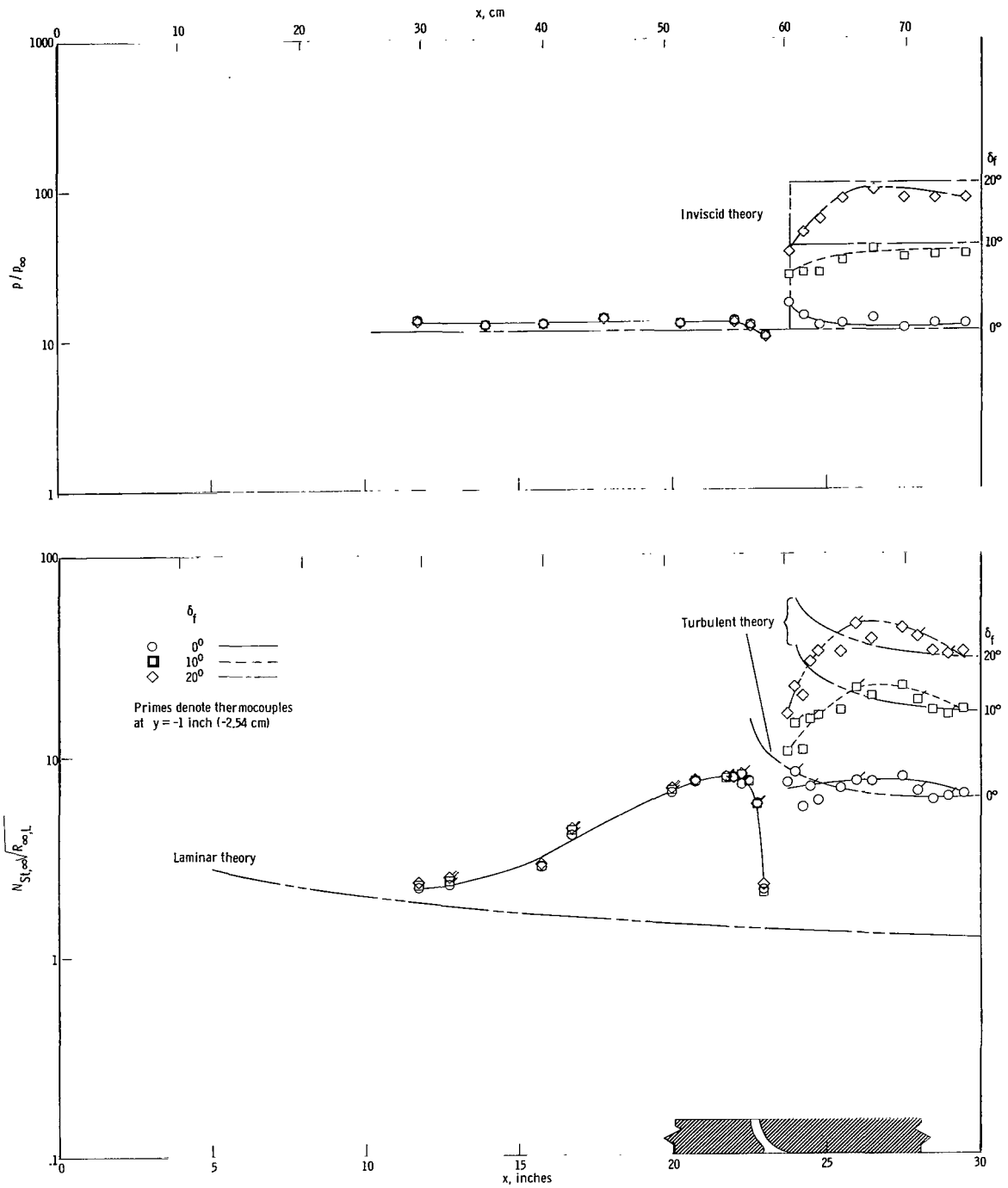

(b) $\varepsilon/r_1 = 0.208$.

Figure 12.- Concluded.

NASA-Langley, 1968 —— 1 L-5733

NATIONAL AERONAUTICS AND SPACE ADMINISTRATION
WASHINGTON, D. C. 20546
OFFICIAL BUSINESS

FIRST CLASS MAIL

POSTAGE AND FEES PAID
NATIONAL AERONAUTICS AND
SPACE ADMINISTRATION

"The aeronautical and space activities of the United States shall be conducted so as to contribute . . . to the expansion of human knowledge of phenomena in the atmosphere and space. The Administration shall provide for the widest practicable and appropriate dissemination of information concerning its activities and the results thereof."

—NATIONAL AERONAUTICS AND SPACE ACT OF 1958

NASA SCIENTIFIC AND TECHNICAL PUBLICATIONS

TECHNICAL REPORTS: Scientific and technical information considered important, complete, and a lasting contribution to existing knowledge.

TECHNICAL NOTES: Information less broad in scope but nevertheless of importance as a contribution to existing knowledge.

TECHNICAL MEMORANDUMS: Information receiving limited distribution because of preliminary data, security classification, or other reasons.

CONTRACTOR REPORTS: Scientific and technical information generated under a NASA contract or grant and considered an important contribution to existing knowledge.

TECHNICAL TRANSLATIONS: Information published in a foreign language considered to merit NASA distribution in English.

SPECIAL PUBLICATIONS: Information derived from or of value to NASA activities. Publications include conference proceedings, monographs, data compilations, handbooks, sourcebooks, and special bibliographies.

TECHNOLOGY UTILIZATION PUBLICATIONS: Information on technology used by NASA that may be of particular interest in commercial and other non-aerospace applications. Publications include Tech Briefs, Technology Utilization Reports and Notes, and Technology Surveys.

Details on the availability of these publications may be obtained from:

SCIENTIFIC AND TECHNICAL INFORMATION DIVISION

NATIONAL AERONAUTICS AND SPACE ADMINISTRATION

Washington, D.C. 20546